JOURNAL OF RESEARCH IN ENGINEERING & COMPUTER SCIENCES

Vol. 1, No. 3, August-2023

JRECS

TABLE OF CONTENTS

EDITORIAL BOARD

DISCLAIMER

All the manucripts are published in good faith and intentions to promote and encourage research around the globe. The contributions are property of their respective authors/owners and Applied Sciences Research Periodicals (ASRP) is not responsible for any content that hurts someone's views or feelings. Authors are responsible for if any plegiarism is found in published material.

Journal of Research in Engineering and Computer Sciences
August 2023, Vol. 1, No. 3, pp. 1-10

Analysis of Power Disturbances and Voltage Imbalances in A City in Nigeria

Tanko Kubuza[1], Azodo Adinife Patrick[2], and Woma TimothyYakubu[1]

1. Department of Physics, Federal University Wukari, P. M. B. 1020, Wukari, Taraba State
2. Faculty of Engineering, Federal University Wukari, P. M. B. 1020, Wukari, Taraba State

Abstract:
Investigation of power quality and the impact is necessary for source mitigation and effect attenuation. An analytical study of the electric power system, including data collection and processing on power disturbances and voltage imbalances at various household end-user points, was carried out in Wukari, Nigeria. The range of power disturbances and voltage imbalances at various end-user points were all factored into the experimental design. Subjective and objective approaches were adopted in the data collection using reliable and validated standard devices. The quantitative data analyzed showed power disturbances through abnormal voltage signals and outages. The technical implications resulted in residences' adoption of phase-to-phase connections to the national grid to meet voltage problems at peak load hours, which raised the voltage to an unusable intensity with a high tendency for electrical/electronic gadget damage. This effect challenges sourcing an alternative means of power supply in the metropolis. This study concluded that mitigation techniques are imperative from the national grid supply source and the household users' points.

Keywords: power quality, voltage, electricity, phase, unbalance.

INTRODUCTION

In Nigeria, electricity which is one of the prominent infrastructures essential for proficient successful disposition in modern life suffers a tremendous deficit in terms of power quality disturbances and voltage interruptions. The nexus between the electricity source, distribution system, and the end users supposes an increasingly crucial role in the reliability and efficiency of the power operation cycle [1]. Reliability and efficient maintenance of electrical power performance are very significant for the continuity of the electricity supply. Typically, electricity distribution networks serve a large number of nodes spanning over large geographical areas. Considering the complex structure of power grid connections, the probability that the system will operate to a standard performance level for a specific period, contingent on specified environmental conditions cannot be guaranteed due to various problems including fault occurrences. Fault in power systems due to inefficient and unreliable distribution networks poses a great threat to consumers in different sectors of the nation's economy. The most obvious effect is the series of power outages experienced in every nook and cranny of the country affecting different activities at residential, commercial and industrial levels. While erratic electricity supplies disrupt electric power-based activities, fluctuation of voltages negatively affects the service life of associated electrical/electronic equipment. Better electricity-related infrastructure can, thus, stabilize the efficiency and durability of returns/incomes.

In an electric power distribution system, a steady-state voltage does not exist. The end-users' characteristic demands from the feeding systems or the loading from the distribution points

continually change, and so do the power system adjustment to these changes [2]. The changes and adjustments due to continual load alterations result in voltage variations which may be for a long duration. It can manifest either as over-voltage or under-voltage, depending on specified conditions for which source path for which the electrical current flow [2]. Significant voltage fluctuations, unbalanced phases, and poor power quality seriously impact performance and useful lives of electric equipment. Some electrical/electronic gadgets are adapted with one form of coil windings or another, which, efficient service delivery of these devices dependent, among other things is the supplied voltage balance status.

Power quality as expressed by [2] is given as

$$\text{Power quality} = \text{Reliability} \tag{1}$$

This simply implies that the availability of electrical networks or the grid is always within voltage and frequency tolerances. Imbalance or unbalance in supplied voltage is defined as the maximum deviation from the average of the three-phase voltages, divided by the average of the three-phase voltages and represented as percentage points [3]. The mathematical relationship for voltage imbalance or unbalance without the phase or line angles is given by National Equipment Manufacturer's Association (NEMA) [4].

$$\text{VL\% unbalance rate} = \frac{\mathrm{D_{max}VL_{3ave}}}{\mathrm{VL_{3ave}}} \times \frac{100}{1} \tag{2}$$

Where,
VL% unbalance rate = percentage line voltage unbalance rate
D_{max} = Maximum deviation
VL_{3ave} = Average voltage of the 3-line voltages
Similarly, Institute of Electrical and Electronics Engineers (IEEE) used phase instead of line for the description of the grid connection [4] thus:

$$\text{VP\% unbalance rate} = \frac{\mathrm{VP_{3ave}}}{\mathrm{VP_{3ave}}} \times \frac{100}{1} \tag{3}$$

Where,
VP% unbalance rate = percentage phase voltage unbalance rate
D_{max} = Maximum deviation
VP_{3ave} = Average voltage of the 3-phase voltages

$$\text{Average voltage } (V_{ave}) = \frac{V_{1R}+V_{2Y}+V_{3B}}{3} \tag{4}$$

Where,
V_{1R} = Grid line one coded red line
V_{2Y} = Grid line two coded yellow line
V_{3B} = Grid line three coded yellow line
The percentage imbalance can be expressed as the ratio of the negative or zero sequence components to the positive sequence component [3, 5]. Assuming there is no fault in the electric power system, the vector sum of the sequence voltages for the grids phases or lines must be zero.

$$\bar{V}_{1R} + \bar{V}_{2Y} + \bar{V}_{3B} = 0 \quad (5)$$

The unequal distribution of single-phase loads in a three-phase circuit is the primary source of voltage imbalance (typically less than 2%). A voltage unbalances exceeding 2% in a three-phase system can cause excessive current imbalance, an increase in winding temperature or overheat that is detrimental to the windings. Blown fuses in one phase of a three-phase capacitor bank can potentially cause voltage imbalance. Single-phasing circumstances can cause severe voltage imbalances (more than 5%) [3, 5]. Motors and transformers overheat due to voltage imbalance caused by device induction current imbalance. It is the deviation from the standard value of 220 Volts between three-phase voltages [6]. The evaluation of power quality involves the analytical study of the power system, such as capturing and processing current and voltage strength values at various points of a distribution system [7]. There is scarcely any research on power disturbances and voltage unbalance from the national grid supplied to the residential sector of Nigeria's economy. It is against this background, that this survey was conducted on power disturbances and voltage imbalance in the Nigeria households.

MATERIALS AND METHOD

Study Area

The survey and data collection took place in Wukari town, Taraba state, Nigeria. Wukari town is located between latitude 7°51'N and 8°15'N of the equator and between longitude 9°47'E and 14'E of the Greenwich meridian. It has an area of 4,308 km (1,663 sq. m) and a population of 241,546 at the 2006 census (Figure 1). The neighboring town includes Ibi town, Gindin, Dorowa, and Jootar. Electricity distribution in Wukari town is done by Yola Electricity Distribution Company (YEDC) Wukari business unit.

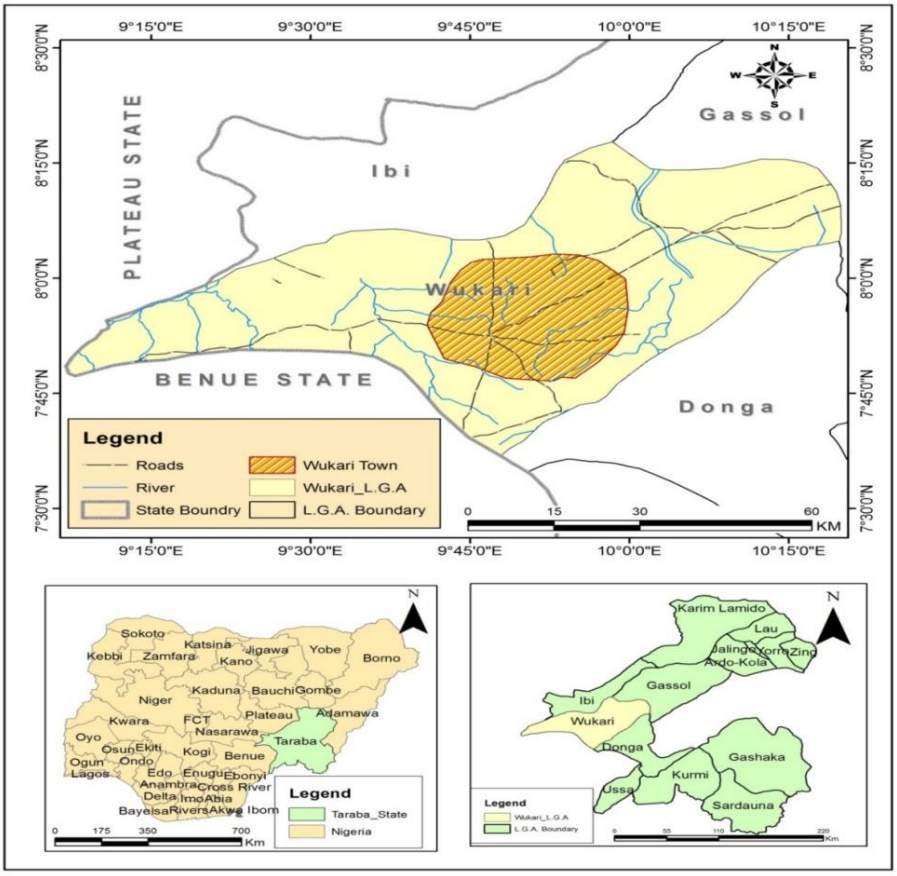

Fig. 3. Map of Nigeria and Taraba State showing the study area (Wukari).

Source: Ministry of land and analysis, Jalingo

The Study Population

The total population of electricity consumers in Yola Electricity Distribution Company (YEDC) Wukari business unit is obtained by summing the total number of consumers in the currently working strata, referred to as k-books, in Wukari; business units (Table 1).

Table 1: Customer Population

K-BOOKS	CUSTOMERS POPULATION
04/14	201
27/35	223
09	60
16/33	422
12	126
08	135
10/11	234
13	112
01/02/03	252
05/06	158
L (Churches and Mosques)	23
M (Commercial areas)	87

(Source: Yola Electricity Distribution Company Wukari Business Unit, 2017)

The total number of customers (population of consumers) is denoted N. The total number of customers in the strata is denoted N*i*.

Where *i* =1, 2, 3, 4, 5, …, 11

$$N = \sum_{i=1}^{n} Ni$$

$$N=N1+N2+N3+\ldots+N11$$

$$N=201+223+60+422+126+135+234+112+252+158+87$$

$$N=2038$$

This is the total population of customers in Wukari business unit besides the churches and mosques. Hence the targeted population was 2038 units.

The study sample for this research was calculated by using Taro Yamane's formula at 95% confidence level (Yamane, 1973). The calculation formula of Taro Yamane is presented as follows.

$$\mathrm{n} = \frac{N}{1 + N(e)^2}$$

Where,
n= sample size required
N = number of people in the population
e = allowable error (%)

Application of Taro Yamane's formula (Yamane, 1973) in study sample determination gave

$$n = \frac{2038}{1 + 2038(0.05)^2}$$

$$= \frac{2038}{5.82}$$

$$= 350.17 \approx 350 \text{ end users'}$$

Study Design

The study focused on the national grid customer population in the Wukari. Subjective and objective approaches were adopted in the data collection for power disturbances originating from consumers' networks, a technicality in national grid connections and implication of power disturbances using a self-developed, pre-tested and validated questionnaire and handheld digital multimeter model M226C. The questionnaire was made up of two main sections, each focusing on a specific aspect. These include location information and power outages. The objective approach focused on electric energy supplied measurement at the end-user point and consumers' networks and devices, which included three-phase loads, unbalanced connections, a lack of adequate neutral wire, no earthing system, and a low circuit breaker rating.

Data Analysis

The data was analysed using a computer software package (Statistical Package for Social Sciences version 16.0) in the form of frequency, percentage, mean, and standard deviation (SD).

RESULTS AND DISCUSSIONS

A representation of the end-users of the national electricity grid revealed that of the three hundred and fifty (350) end-users of electricity targeted by this study, two hundred and nine (209) customers participated, representing a response rate of 59.71%. The outcome of interference emanating from end-user networks and devices was evaluated. These mainly include disturbances due to phase loads, connection imbalances and the lack of a suitable neutral conductor (low circuit breaker rating or grounding system).

There are typically four network lines distributed across the transmission towers. The first above was coded as a red line, the second as a yellow line, the third as a blue line, and the fourth as a neutral line. Due to the three-phase mains connection of three life wires and a neutral conductor, a total of four cables are required from the public power grid to the meter panel on the house wall (Figure 1a). The two-phase grid connection consists of two life wires and a neutral line, i.e. a total of three cables from the utility grid to the meter panel on the house wall (however, no classified connection by the YEDC Wukari business unit). Single-phase, consisting of a live wire and a neutral wire, for a total of two wires connected to the meter board (Figure 1b). The phase-to-phase mains connection is a combination of two lifelines to the meter board with no neutral (safety) wire (Figure 1c).

Figure 1(a) Three-phase connection (b) Single-phase connection (c) Phase-to-phase Connection

The result showed that 86 end-users representing 41.1% of participants, had a single-phase, 53 end-users representing 25.4% of participants, had a three-phase, 45 end-users representing 21.5% of participants, had a phase-to-phase wire connection, with 25(12.0%) unspecified others.

The three-phase supply should be distributed evenly and reasonably across the three-phases. Single-phase loads connection of different demand capacities and characteristics, as well as power consumption to a three-phase electric power supply system, will cause unbalanced voltages distribution of phase or gridline voltages at the point of the power supply and unequal currents flow in the three-phase power circuits [9].

In addition, unbalanced phase voltage distribution in the three-phase supply voltages can create negative sequence components, thereby inducing extra power losses with undesirable currents and voltage drop in neutral conductors [9].

The power quality relies on the electric power availability from the national grid within voltage and frequency tolerances. Unbalanced distortion is one of the power qualities factors in determining the energy efficiency of the power distribution system.

Measuring transformer load from single-phase loads has shown that all single-phase loads are potential sources of unbalanced distortion [9] with adverse effects on the electric power distribution system, such as unbalanced 3-phase voltages.

From the analysis of the voltage unbalance in the three-phase grid connections using the formula stipulated by the National Equipment Manufacturer's Association (NEMA) and the maximum allowable unbalance tolerance of 2.0%, there were several unsatisfactory grid connections unbalanced in the metropolis (Table 2). The absence of proper neutral lines was also observed in several participant households. These contributed to the witnessed voltage fluctuations.

Table 2. Voltage strength values at various points of power distribution system

Districts	Voltage strength values		Remarks	
	Off-peak hour	Peak hour	Off-peak hour	Peak hour
N1	1.61%	4.34%	Satisfactory	Unsatisfactory
N2	14.40%	6.23%	Unsatisfactory	Unsatisfactory
N3	2.80%	1.00%	Unsatisfactory	Satisfactory
N4	6.40%	2.30%	Unsatisfactory	Unsatisfactory
N5	1.46%	3.21%	Satisfactory	Unsatisfactory
N6	4.10%	3.65%	Unsatisfactory	Unsatisfactory
N7	8.00%	3.37%	Unsatisfactory	Unsatisfactory
N8	3.30%	2.29%	Unsatisfactory	Unsatisfactory
N9	4.61%	3.48%	Unsatisfactory	Unsatisfactory
N10	4.15%	1.57%	Unsatisfactory	Satisfactory

Also, from the analysis, welders were found near many households. This intermix in the land use development planning in the metropolis results in a fluctuation in the power supply since the most prevalent causes of voltage fluctuation are electric arc furnaces and welders. Comparing the intensity of a voltage flicker to the sensitivity of human visual perception revealed that a high response (95.2 per cent) might generate voltage fluctuations or lamp flickers by exhibiting continuous, rapid variations in the load current magnitude [5]. Continual unpredictable voltage sags and swells can cause sensitive equipment to malfunction, overheat the equipment, and shorten its life [5]. Under voltage is defined as a drop in RMS ac voltage below 90% at the power frequency [5]. The power supplied by the national grid does not satisfy the electric power need of 86.8% of participant households. The reason ranges from high voltage (3.8%), low voltage (27.3%), power outages (29.7%) and unspecified others (39.2%). High voltage is predominantly observed in the night seasons (55.5%), whereas low voltage becomes the issue in the daytime (63.2%). Validation of the participants' observation was the physical measurement obtained at each household unit. Analysis conducted regarding the nominal standard value of 220 Volts stipulated for electrical/electronic gadgets in Nigeria, and values considered as under and over-voltage as decrease or increase beyond 10% in the RMS ac voltage from the nominal value [5], Figure 3 showed that at off-peak periods, the voltages were overvoltage for the three grid lines over 198 – 242 volts range which make them prone to the destruction of tools used by the households. At peak load hour, the residences have the options of switching to a grid with nominal voltage, but districts N2, N3 and N6 that have all the grid voltages not more than the standard value.

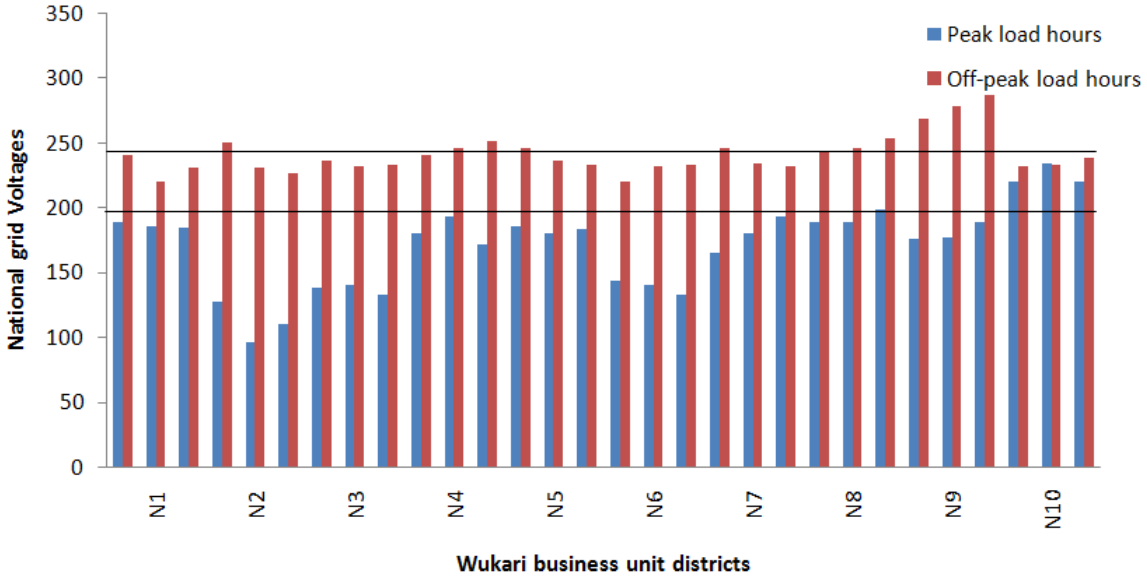

Figure 3. Average voltage status on three-phase grid connection

Single-phase connection showed under-voltage at peak load hours, which affects the users. However, at off-peak hours, it was found that the voltage increased to a range of nominal usable voltage with slight overvoltage in district N4 and overvoltage in district N9 (Figure 4). To enhance the supplied voltage during the off-peak period, some households adopted a phase-to-phase connection that increased the available voltages to a non-useable level (overvoltage) (Figure 5). Higher or lower than nominal voltage or current can cause certain types of equipment to malfunction or be damaged, as is well known. [7]. 80.4% uses electric power stabilizer in their utility connections, while 19.1% of participants do not use a stabilizer. 51.4% used a stabilizer in connection. While 48.6 did not use a stabilizer in the grids.

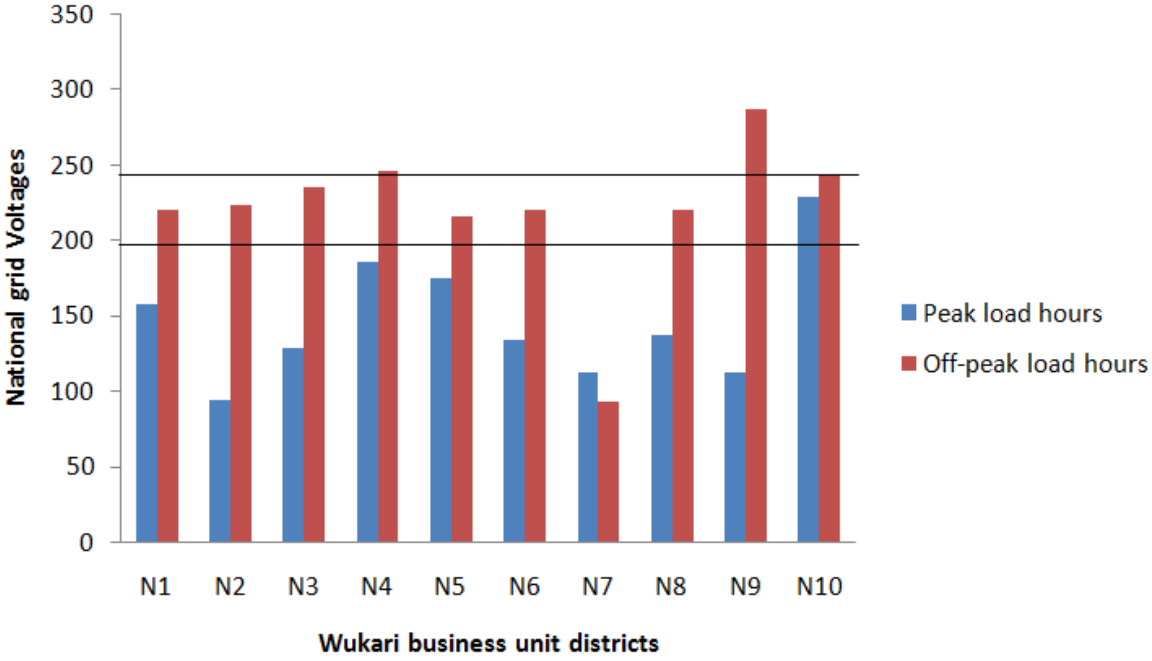

Fig. 4. Average voltage status on single-phase grid connection

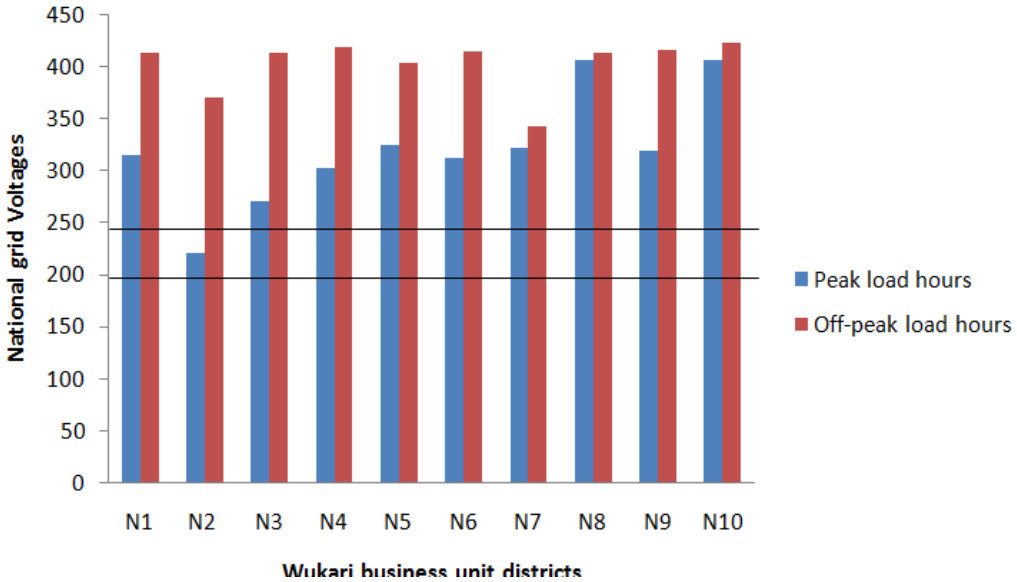

Fig. 5. Average voltage status on phase-to-phase grid lines connection

Power quality has a direct impact on electrical equipment and diverse systems because power interruptions cause equipment damage and poor system performance. Power quality testing should be done frequently with high-sensitivity equipment to maintain optimal performance. It is established that higher or lower than nominal voltage or current can cause equipment to malfunction or be damaged [7]. The electricity supply in Nigeria is not only unreliable but also of poor quality. There is no information on the state of the Nigerian power system's power quality [7].

A power outage is a complete power loss caused by faults and accidents [5]. Mitigation to power outage problems is to seek an alternative means of power supply such as a standby electric power generator. One hundred and thirty-one (131) participant households have alternative power supply means, out of which 97.1% are predominantly generators. This proportion of the participants adds to 81% (130/160) million Nigerians who generated their electricity through alternative sources to make up for irregular power supply [10]. Consequently, the result agreed with the observation made by Azodo [11] in a southwestern city in Nigeria.

CONCLUSION

Electric power distribution from the national grid within the acceptable voltage and frequency tolerances to the end-user is achievable. The power disturbances and voltage imbalance sources analysis in this study showed that end-users' characteristic demands from the feeding systems or the loading from the distribution points, type of grid connection and presence of high-power demand equipment such as welding process contribute to the witnessed voltage fluctuations in the metropolis. Inadequate power quality through under-voltages from the feeding systems was predominantly observed at peak load hours but changed to over-voltage during off-peak hours. The role of the end-users in the power quality demands the engagement of the local electric utility company or a highly skilled electrician for appropriate grid connection and notification of relevant authorities on power issues perceived concerning the supplied power. But, then, a substantial supply system can significantly reduce the severity of voltage fluctuation, which concerns the electric utility company in the area.

REFERENCES

[1] Adejumobi, I. A. and Olanipekun, A. J.(2009). Software application for electrical distribution system x studies: box-Jenkins's methodology. *Pacific Journal of Science and Technology, 10*(2), 377-387.

[2] McGranaghan, M. (1998). Power Quality Standards. Electrical Contractor Magazine, Electrotek Concepts, Inc. Retrieved Auugust 7, 2017, fromwww.pqmonitoring.com/papers/Power Quality Standards/overview.PDF

[3] Gonen T. – Electric Power Distribution Engineering, Third Edition. CRC Press Taylor and Francis group, Boca Raton London New York, 2016

[4] Pillay, P. and Manyage, M. (2001). Definitions of voltage unbalance. *IEEE Power Engineering Review, 21*(5), 50 – 51.

[5] Fathi, H. M. E. (2012). Power quality assessment. PhD Thesis, Al-Azhar University Cairo, Egypt.

[6] Kazibwe, W. E., and Sendaula, M. H. (1993). *Electrical power quality control techniques*. Springer Science & Business Media. International Thomson Publishing Berkshire House, Hogh Holborn, London.

[7] Ogunyemi, J., Fakolujo, A. and Adejumobi, I. A. (2012). Power quality assessment in Nigerian distribution network. *EIE's 2nd Intl' Conf.Comp., Energy, Net., Robotics, and Telecom, eieCon2012*, 103 – 111.

[8] Yamane, T. (1973). Statistics: An introductory analysis. 3rd Edition, Harper and Row, New York.

[9] Martin, I. and Kwok-Tin, W. U. (2003). Standards of power quality with reference to the code of practise for energy efficiency of electrical installations. Energy Efficiency Office, Electrical & Mechanical Service Department, Retrieved June 18, 2017, fromhttp://www.emsd.gov.hk/filemanager/en/content_764/EEC_harmonic.pdf

[10] IseOlorunkanmi, J. I. (2014). Issues and challenges in the privatized power sector in Nigeria. *Journal of Sustainable Development Studies, 6*(1),161-174.

[11] Azodo, A. P. (2014). Electric power supply, main source and backing: A survey of residential utilization features. *International Journal of Research Studies in Management, 3*(2), 87-102

Journal of Research in Engineering and Computer Sciences
August 2023, Vol. 1, No. 3, pp. 11-14

Easter Thoughts on Artificial Intelligence: A Christian Approach

Peter G. Gyarmati

Abstract:
A technique based on today's results of science is becoming dominant in almost all fields under the name Artificial Intelligence (AI). At Easter, some Christian-minded people gathered to discuss the impact, advantages, and dangers of Artificial Intelligence. The debate centered around the preservation or reinterpretation of the dogma of creation. If the dogma is valid - God is the only creator - then the creation of Artificial Intelligence cannot dominate man - there is no danger. But man is creative and has always 'created' things throughout his history that have no example in God's creations. Rather able to create such machine that may rule over the man? The danger does not lie in this, but in the bad intention, which is also human. What possibilities do we have for recognition and protection? This study deals with the relationship between Humans and AI from a scientific, rather than a technical, aspect.

Keywords: Artificial Intelligence, Machine Learning, Human Intelligence, Christian Science, Formal Logic, Automatic Decision, Danger.

Easter was the time for a Christian-spirited discussion about the intellectual technique that concerns the whole world, about Artificial Intelligence.

- Through Artificial Intelligence, man is able to produce creatures, which is only God's ability.
- God created man in his own image, but endowed him with 'only human abilities' - not divine ones.
- Creation is a divine ability, even angels and saints cannot do it.
- The world must be saved from the harm of Artificial Intelligence. Limits and boundaries must be introduced!
- such different opinions were expressed.

Starting from the Christian faith, we can quote St. Thomas Aquinas, according to whom the ordered world - our physical, metaphysical world - can be known, and above which 'the world of supernatural truth is hidden' and cannot be penetrated by thinking. The divine revelation radiating from here can only be accepted, because it is beyond human reason, but not unreasonable. Man has free will only in his own world. According to St. Thomas Aquinas both the good-ethical action and the bad-unethical action have the same origin, the free will.

We know and see many examples of this: man-made destructions, the rivalry production of weapons aimed at everyone, methods that incite people en masse against each other. And all of these have unlimited applications. The entire human world can be destroyed with these, but they haven't done it yet. Although they are capable of inflicting any kind of pain and suffering on humanity, it has always been followed by resurrection and new life. This is the will and intention embodied by God in Jesus! If it didn't happen like this once, then everything would be over and any thought would cease to exist.

Man is therefore able to destroy his own world, even several times, but even then, he is not able to penetrate into the supernatural.

Some may think otherwise: let's find, create another world - free will allows - for ourselves and then everything we have now will become redundant and can be destroyed. Space travel is one such intention with its many experiments.

If, according to predestination, God's created world is eternal, then man cannot destroy it. If those with weapons of mass destruction knew this for sure, then they could use them freely, the Earth, nature would be preserved and they would be the survivors, that is, evil can win, good is destroyed - various opinions were expressed.

Is this the way? Any thought can become an action, because free will gives it?
Let us examine the 'softer' direction, where man lives in the 'world of physical and metaphysical knowledge' and intends to keep it. However, thinking cannot penetrate the 'supernatural truth hidden above'. Even if we accept this thousand-year-old dogma, the question still arises: could people have managed to penetrate there just by chance? They must have entered, seen, heard, dreamed, imagined and returned! Because we know about such people: Buddha and Muhammad also claim it, and then there is, for example, Prometheus, Archimedes, Leonardo Da Vinci, Mary Curie, Tesla. Each of them brought something to humanity that can only be seen and understood from outside our own world (!). So, it is possible. Where is the barrier? As believers, we know only one thing: the wrath of God, who has enough of it - no more. But, at Sodom, God limited himself, there is no more anger and then the free will and chance remained!

The unethical actor - the evil one - can destroy freely, but he cannot destroy God's creation, there must be a limit and this is the preservation and maintenance of his own existence. So, there must also be divine predestination in evil.

What about ethical actors? In order to make his life better, more comfortable and richer, based on the principle of free will, he creates more and more skillful, meaningful and independent tools. Artificial Intelligence is the result of this development, which even in its rudimentary nature exceeds these intentions and seems to be a fundamental tool of the world of creation. And this contradicts to the dogmatics of creation.

If man is not able to penetrate the world of the supernatural truth of St. Thomas, then Artificial Intelligence does not contain any danger from this point of view, it is not able to create! Perhaps those who entered with divine permission brought it with them, then it obviously has a divine limit. From another point of view, over the results the AI can have many kinds of dangers. This question does not belong here.

So, we have no business with him, he cannot create, there is no danger! If we were to assume it, then the dogma of creation would be destroyed!

But does this dogma still exist? Are only a lot of people talking about it, referring to it, applying it, even though it has long since fallen into disuse? Then is this dogma valid for people of other religions or for atheists? Or perhaps universal, i.e., independent of faith?

By this way, the question of whether creation is possible in the world of man comes into a completely different light.

If the dogma of creation were still valid and universal, then there is no danger, there is nothing to draw attention to! It is unnecessary and surplus to formulate limits and boundaries!

I don't want Artificial Intelligence and other similar important issues to fall into the world of dogmatics, because I think the matter is not that 'simple'. Let's try to formulate what creation is and how human action relates to it.

1. It comes from the Creation; our entire world is a creation - we think and believe it is a divine creation. You cannot know more than this even without faith, all ideas and assumptions are therefore also faith.
2. If there is something in this world that was not there before, which has no origin, then according to the theory, God created again?
3. The most fundamental invention of humanity, which does not exist in nature independently of man, is what if not creation? Man created the wheel, the bearing and axle dual! So, is man a creator? It may have been suggested by God, or it may have been an accidental passage, but it is certainly human!
4. And man has created many other things: bridges, houses, steam engines, airplanes, medicines, plastics, viruses, computers, robots, artificial intelligence!
5. The dogma of creation has fallen! And the cause is not the bad, or sin. It stems from ethical act even in the Saint Thomas's sense!
6. We can say the dogma is invalid, not divine will! Or maybe God has changed? I wonder why, what could be his reason for it? Maybe it was influenced by man? The answer the only one: we are constantly penetrating the vault of supernatural truth.

The core of our thinking is that what can be proven logically is logical and conversely, if something is logical, then it can be proven logically!

If God's existence could be proven, then his actions are logical, so they can be imagined. And then man can access it, there is no supernatural truth that cannot be penetrated by thinking! So, man is able to create, even ethically. And those who can do this can also destroy. God did it too and is limited only by his vow of Sodom. Or not exist for a long time, left for somewhere: over the black-hole?

This does not bother the non-ethical people in their actions either, so there is a danger! The danger is great, the destruction of humanity is a real possibility. Prevention cannot be solved with limits, God set the limit for himself: I will never bring a flood to Earth again. Only with more power would we be able to limit the danger makers. Even this way would take an unheard effort and risk.

But there is no such power, then there remains the chance of self-limitation, as with God. The question is, those who cause danger have such a quality? Maybe. So, we have to use our brain, as a tool that shows that dominance is not homogeneous and cannot exist in all space and time. There are weak points, not a few.

1. Among others, there are believers among those who cause danger, their lives are also finite, and in order to survive, they too must ensure the living conditions of their descendants.

2. Then those who cause the danger are divided - they are rivals in capitalist competition and threaten each other with their destructive tools.
3. They also develop prevention tools and even negotiate with each other.
4. These are roughly the areas of self-limiting tendencies.

External Factors

1. The background of the prosperity and power of those who cause the danger is the ability and action of their empire. Any disturbance in the realm will limit them. Disturbance is poverty, crisis, rebellion, resistance, revolution, destruction, victory, defeat.
2. Their creation lies in union. We know that two people who join their forces are more powerful than the sum of their individual strengths; because they can, for example, protect each other's backs if they stand up like that. A well-known saying about getting married: until now there have been two of you and me; from now on we are three: you, me and us. Well, that's the power of union.

Artificial Intelligence has already, here at its umpteenth flare-up, once again achieved significant results: finally acceptable quality translation of human languages into one another, video technology, shape recognition, data processing and increasingly accurate interpretation, creation of more and more versatile and reliable robots and machines, expanding the possibilities of relationships between people, to list only a few important areas, and subsequently the organization and operation of all this is the task of Artificial Intelligence. This is all Saint Thomas ethical action!

The danger still exists! precisely that all these results can be used for non-ethical action as well! Those who cause danger do this to achieve their own interests and goals, if they can achieve it in this way. High-quality language translation is an increasingly accurate and therefore automated means of eavesdropping on the observed. Video technology, shape recognition, and data processing are excellent tools for observing and discovering people, opponents, and enemies. Robots have become excellent combat tools; they are already regularly used in today's wars. We see the destruction that drones do with great safety and precision. It is slowly becoming commonplace that people's affairs are handled by the authorities with robots and automata: zero tolerance becomes complete. These are examples of St. Thomas' unethical actions.

Without any more explanation, it is clear that the problem is not with Artificial Intelligence, but with its application methods. Just as it happened with all the discoveries of humanity so far.

We were/are unable to prevent destruction by weapons, colonization, exploitation, corruption, election fraud, misleading news, intentional air pollution, potato bugs, cultivated viruses, climate change, unethical actions in the St. Thomas sense.

- The cooperation and opposition must therefore not be directed against the means, but against the unethical act and the possibility of it!
- János Neumann formulated it in the fifties of the last century: 'there is no medicine against development; the solution lies in the cooperation of man and machine'.
- And - I'll add this - the initiator of the collaboration can only be the man, and the ethical actors should never let this out of their hands again!

Journal of Research in Engineering and Computer Sciences
August 2023, Vol. 1, No. 3, pp. 15-32

Estimation of Skin Cancer with Integrated Extended Convolutional and Recurrent Neural Network Techniques on Image Dataset

Chin-Ling Chen[1,2], Asadi Srinivasulu[3], Ravikumar, C. V.[4], G. V. Ganesh[5], Goddindla Sreenivasulu[6], Karuna, Y.[4], Yong-Yuan Deng[2]

1. School of Information Engineering, Changchun Sci-Tech University, Changchun 130600, China
2. Department of Computer Science and Information Engineering, Chaoyang University of Technology, Taichung City 413310, Taiwan
3. Data Science Research Laboratory, Blue Crest University College, Monrovia, Liberia-1000
4. School of Electronics Engineering, Vellore Institute of Technology-Vellore, India
5. Department of Electronics and communication engineering, Koneru Lakshmaiah Education Foundation, Vaddeswaram 522502
6. Department of Biotechnology, Prathyusha Engineering College, TN, India

Abstract:
Skin cancer is the most common and possibly fatal type of cancer that necessitates early detection through the deep-learning method. Machine learning approaches such as random forest and Naive Bayes are used to identify skin cancer. Numerous studies comparing the efficacy of Artificial Intelligence (AI) based models for automated skin cancer classification to that of human experts have laid the groundwork for the effective deployment of AI-based tools into clinical pathological practice. The detection of skin cancer using Naive Bayesian display an accuracy of 86% and the random forest method exhibits an accuracy of 87%. To improve the accuracy, an automatic skin cancer detection using an Extended Convolutional Neural Network (ECNN) technique is proposed with 12 nested processing layers, which enhances skin cancer diagnostic and detection accuracy. The ECNN network and extended Recurrent Neural Network (ERNN) display an accuracy of 94.02% and 87.32%, respectively. These investigations assess the clinical relevance of three important aspects of the existing research on melanoma reader studies: test set characteristics (composition, and out-of-distribution dataset), experimental or clinical data (metadata), and clinical symbolism of the participants. These aspects are tested set characteristics (composition, and out-of-distribution dataset); experimental or clinical data (metadata), and clinical symbolism of the participants. The search included digital biomarkers, histology, whole slide imaging, deep learning, melanoma detection, and skin cancer categorization. The results suggest that ECNN and ERNN models are more resilient and dependable when compared to existing transfer learning models.

Keywords: Skin Cancer Dataset, Machine Learning, CNN, Deep Learning, RNN, ECNN, Health Data Analytics, ERNN, Artificial Intelligence.

INTRODUCTION

In common parlance, cancer refers to a wide spectrum of disorders that affect the human body. The sickness is essentially a weird cell development that attacks neighboring cells and spreads to organs of the body; this contact is referred to as metastasizing. Cancer is the world's second greatest cause of mortality, killing around 9.6 million people or one out of every six deaths (Bray et al., 2018). Skin cancer has recently become the most common and dangerous type of cancer

detected in humans. It can take many distinct forms, counting melanoma, squamous cell carcinoma, and basal cell carcinoma, the latter of which is difficult to diagnose. Melanoma and non-melanoma skin malignancies have become more frequent in recent decades. Each year, there are between 2 and 3 million and 132,000 incidences of non-melanoma skin cancer worldwide. According to the Skin Cancer Foundation Statistics (SCFS), one in every five Americans is affected by skin cancer. Melanoma is the 19th most common malignancy in both men and women. In 2018, there were roughly 300,000 incidences of skin cancer. Non-melanoma skin cancer is the fifth most frequent type of cancer, affecting one million men and women globally (Nahata & Singh, 2020).

Because of their similarity, cancer detection and diagnosis are the most difficult for medical experts. Skin cancer cannot be noticed with the naked eye since it first starts as a little mole (Kadampur & Al Riyaee, 2020). Information Technology (IT) tools play an important role in disease diagnosis. The advancement of IT allows for advances in health care in disease diagnosis, management, and support. Improved decision support systems that are coupled with evidence-based medicines also help clinicians with the diagnostic process (Krive et al.,2015). Numerous researchers have employed IT to identify and diagnose skin cancer. Some of them used Machine Learning Techniques such as Naive Bayes, Random Forest, Agent Technology, and Neural Networks (Mahesh, 2020).

Deep Learning Technologies, such as Probabilistic Neural Networks (PNN), Artificial Neural Networks (ANN), and Convolution Neural Networks (CNN) on the other hand, has demonstrated the highest performance in skin cancer identification and diagnosis (Salvi, Acharya, Molinari, & Meiburger, 2021). Cancer is a serious threat to human life. It may risk human life on occasion. Various types of cancer may harm the human body and skin cancer is one of the deadliest. Smoking, drinking alcohol, allergies, becoming sick, acquiring viruses, being active, altering the environment, being exposed to ultraviolet (UV) light, and other factors contribute to it. The sun's UV rays can damage DNA within skin cells. Unusual bodily swellings can potentially cause skin cancer. According to Dorj, Lee, Choi, & Lee (2018), Actinic Keratoses, Basal Cell Carcinoma, Squamous Cell Carcinoma, and Melanoma are the four most common types of skin cancer. Pacheco and Krohling (2019), predict that skin cancer will account for one out of every three new cases of cancer. Skin cancer prevalence has steadily increased in the United States, Canada, and Australia over the last few decades.

Malignant Melanoma (MM) accounts for around 75% of all skin cancer deaths although accounting for only 4% of all skin malignancies. Early discovery and diagnosis are important for the survival of those who are afflicted [1].

On the other hand, because of the physical overlap between MM and atypical melanocytic nevi, early identification may be difficult. Despite the dermo copy enhances diagnostic accuracy over naked eye examination [2, 3], sensitivity levels above 80% are uncommon even for professionals. Aside from that, there is considerable diversity dependence on professional experience and training [4]. When an MM is suspected, a skin sample is conducted to allow for histological analysis. Even though the histological investigation is currently recognized as the gold standard for identifying skin cancer it is labor-intensive, time-consuming, and occasionally inconclusive. Individual pathologists' MM classifications varied by up to 25% among studies [5, 6].

LITERATURE SURVEY

Huge research has been conducted to discover and diagnose problems. The greatest ones pertinent to the present work were exhibited and discussed in detail. Earlier melanoma skin cancer hybrid approach for assessing worrisome lesions has been developed by Daghrir, Tlig, Bouchouicha, and Sayadi (2020). The suggested system is based on three prediction methods: CNN and two machine classifiers. The color, boundaries, and texture of the skin lesion are used to train the machine-learning classifier. Following that, these strategies are integrated to retrieve their presentations via a majority vote. The International Skin Imaging Collaboration (ISIC) dataset, which contains 640 images, was used to assess the functionality of the proposed system. The results show that when these three methodologies are combined, they attain the highest level of accuracy, which is 88.4%. Ulzii, as well as others, CNN, according to Dorj, Lee, Choi, and Lee (2018), is a smart and fast skin cancer classification system.

Furthermore, support vector machines (SVM) and error-correcting output coding were used to classify skin cancer (ECOC). Kaggle photos of skin malignancies in color RGB mode (red, green, blue) were collected and utilized to evaluate the performance. A specific set of photos contains noise from tools and other organs. The findings can be improved by trimming these photographs. The proposed algorithms were put to the test on 3753 photos of four different forms of skin cancer. The implementation findings show that the maximum average accuracy values are 95.1 percent. Melanoma is a type of skin cancer that results in the formation of malignant skin tumors. Skin cancer is detected using dermatological photos.

Machine learning based on a high-performance image detects skin cancer with high accuracy (Srividhya, Sujatha, Ponmagal, Durgadevi, Madheshwaran, et al., 2020). More features can, however, be retrieved to improve the model's accuracy, and the sensitivity is more varied. Hoshyar, Al-Jumaily, &Hoshyar (2014) developed a strategy for improving skin cancer diagnosis accuracy by using image processing techniques. They were unable; however, to describe precise cancer detection methodology. Another study's author offered an architecture-driven model for skin cancer diagnosis that used a Deep Learning (DL) algorithm. Because DL based on a model-driven architecture can be developed so quickly and the model can predict the outcome in the same amount of time. It improved its identification of skin cancer (Kadampur & Al Riyaee, 2020). However, real-time connection with medical pictures is essential for the technology to aid the medical industry.

According to the findings of Esteva et al. [8], a CNN-based deep-learning image classifier performed better than 21 clinical and dermoscopic dermatologists with board certification image classification. Because of this, the review was carried out by using the databases PubMed, Medline, and Science Direct for the English-language publications that were reviewed by peers and published between 2017 and 2021. (The search keywords were accessed for the very last time on February 17, 2021) Deep learning, melanoma detection, skin cancer classification, Whole slide imaging, histopathology, and digital biomarkers were produced by combining the following search terms. Table 1 gives a comprehensive overview of the search strategy.

The search results were reviewed by hand. According to literature provide a full summary of the PRISMA-compliant systematic search technique. Only publications that matched the requirements for inclusion were chosen. At first, the only study considered for inclusion was that which involved direct comparisons of AI classifiers with human professionals. This was because these methods better highlighted the potential value of AI-based classifiers in clinical

pathological practice. Procedures that did not involve comparisons were left out of references [9-12]. In addition, only trials in which MM had a diagnosis were taken into consideration. Because Merkel cell carcinoma (MM) is the subtype of skin cancer that is linked to the highest mortality rate, it was considered research that entirely discounted the possibility of having Merkel cell carcinoma.[13]. In the end, the research that was primarily concerned with the classification of diagnostic criteria was only considered. Prognostic indicators such as therapeutic response and long-term survival were eliminated after painstaking analysis based on references [14-15]). Only peer-reviewed articles were used to retrieve the data. Two reviewers separately assessed the data's quality.

SYSTEM METHODOLOGY

Existing System

CNN and RNN are two separate algorithms used by deep learning researchers [21, 22]. Despite their extensive application and great outcomes, these tactics have the following limitations. The caveats of CNN and RNN techniques are shown in Table 1.

Proposed System

The methodical collection of relevant literature for this investigation was accomplished using the methods outlined below. To get things started, we gathered a list of research repositories, conferences, and journal papers related to computer science and digital humanities. Although many other places and fields, such as law, security and shadowing, and text dispensation, can fulfill these comprehensive supplies, we believed that our choices would be sufficient as a starting opinion for giving contemporary dialogues on the topic at hand.

We have compiled and organized all the releases for these websites, starting with the most recent and working backward in time by six years (inclusive of 2015-2020). 2015 was selected as the starting year for this project for two reasons. On the one hand, recent advancements in the utilization of known as deep learning or neural networks have significantly driven the current iteration of AI [19]. The ImageNet Large Scale Visual Recognition Challenge in 2012 was won by convolutional neural networks, which were 41% more accurate than their non-neural competitors (ILSVRC). Though neural network research has been going on for decades, it has only recently acquired general acceptance. Starting the emphasis in 2015 looked like the ideal moment to do so given the amount of time that would be required for these enhancements to affect a distant market such as documentation. In addition, because we wished to concentrate on recent disagreements and prospective perspectives, we investigated the possibility of employing modern AI [11-12]. Prior to this date, a cursory review of journals was sufficient to support our judgment. This research seeks to avoid the drawbacks of current CNN-RNN algorithms [30], as stated in Table 1, Table 2 describes how the suggested model enhanced prototype combines the CNN-RNN method to build a hybrid model with the following benefits [18].

Table 1: The Caveats of CNN and RNN Techniques

CNN	RNN
▪ Less precision and accuracy	▪ Small-data object detection is inefficient.
▪ The error rate is high.	▪ Good for predicting data labels, but not for segmentation
▪ High level of time complexity	▪ Less precision and accuracy
▪ Incapable of dealing with large amounts of data	▪ prone to errors

Table 2: Implications of the ECNN and ERNN approaches proposed

ECNN	ERNN
▪ High precision, low accuracy	▪ Easily detects small-data objects
▪ Relatively low error rate	▪ Excellent for data separation and forecasting.
▪ Reduced time complexity	▪ Precision and accuracy are quite high.
▪ Handles large amounts of data	▪ Less prone to errors

Input Data

The experimentation of this projected building was based on a dataset of 660 CT scan pictures from the Kaggle source https://www.kaggle.com/datasets/kmader/skin-cancer-mnist-ham10000). Figure 1 depicts a portion of the input dataset that was segmented into two categories during the experimental stages: training cases and testing cases. These categories were determined by the results of the previous stage.

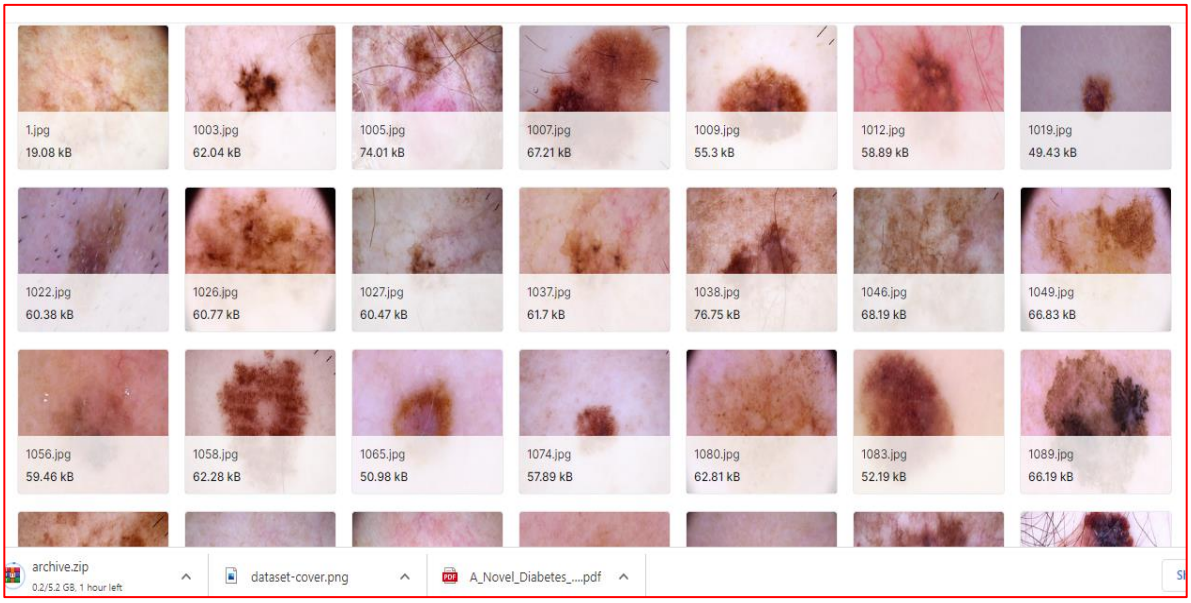

Fig. 1: Skin Cancer Virus Image Dataset in Kaggle Database

ECNN-ERNN Workflow Diagram

Figure 2 and Table 3 depict the suggested architecture for employing the ECNN algorithm to predict and detect skin cancer, which accepts a dataset from the Kaggle public repository and preprocesses it using many layers of the extended CNN approach.

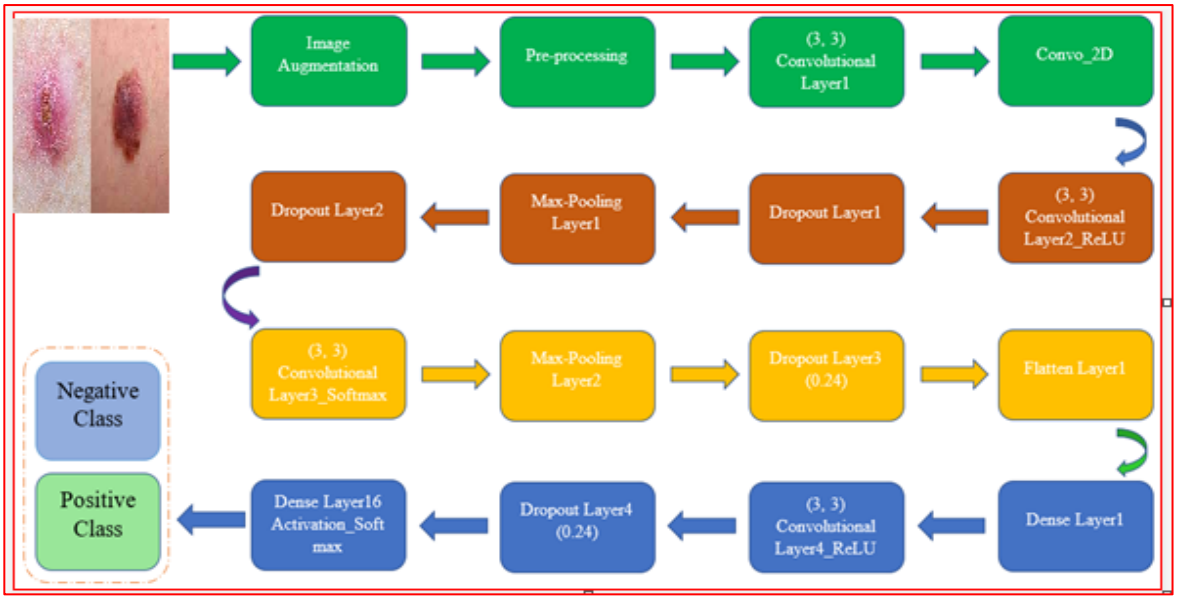

Fig.2: The suggested model's workflow diagram is based on ECNN

Table 3: The ECNN approach's algorithm steps

Step 1: Import required libraries
Step 2: Pre-processing of the dataset
Step 3: Combined CNN with Extended Neurons
Step 4: Perform 10-folded cross-validation with 2 classes
Step 5: Import Keras deep learning library with all supported libraries
Step 6: Reset all parameters of ECNN
Step 7: Enhance the ECNN part and regulation of the loss calculation function
Step 8: Enhancement of yield part of 10-folded with 2 classes
Step 9: Accumulate the ECNN parameters
Step 10: Adjusting the ECNN in the preparation of model
Step 11: Load the Skin Cancer disease infection image dataset
Step 12: Predicting the infection severity by classifying the dataset into 2 classes
Step 13: Outcome of the trained model and stop the model

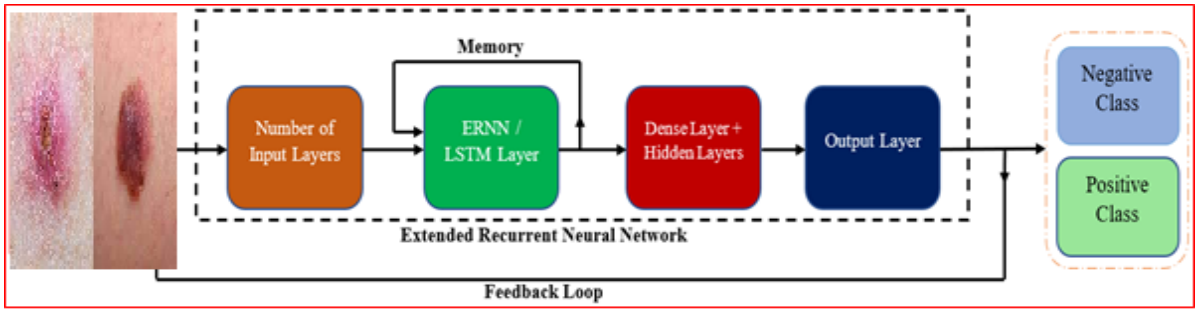

Fig.3: The suggested model's workflow diagram is based on ERNN.

Figure 3 depicts the suggested architecture for ERNN-based prediction and detection of skin cancer. Using ERNN/LTSM layers, dense layers, and hidden layers, the prototypical was qualified to predict the optimistic and undesirable classes in the provided dataset and then evaluated for precision, accuracy, and error ratio [26]. A wide range of DL models, including individual and assisted learning, have been proposed to solve several difficulties [27]. The nodes in the output layer are responsible for determining the probability of each label. Most of them are used for language learning, visual organization of images, and object recognition. In the relapse tier, activation activities are distributed across three fully interconnected layers containing 4095 hidden hubs. In this model, the projected thickness in millimeters is linked to the yield strength. The final yield layer is merely a single hub that has not been affected by the following factors:

Data Pool:
The challenging dataset comprised 660 rows and four columns, whereas the training dataset contained 660 images. The training dataset also contained 660 rows. The training database has 660 CT-scan photos spread throughout its four different columns.

ECNN-Layer:
A necessary component for the formation of neural networks. This is the most common and straightforward application of information levels [33].

ERNN-Layer:
It is a layer of recurrent neural systems in the deep learning approach. In this exploration article, this layer was reached out to address and demonstrate sequential and time-autonomous concerns, as well as well-being information forecast.

Pooling Layer:
Following the convolutional layer, another layer known as the pooling layer is added. Specifically, after applying a non-linearity, such as ReLU, with respect to the constituent maps produced by a convolutional layer; a model's layers, for instance, could look like this: It is necessary to enter image data [34–37].

ReLU-Layer:
If the performance is positive, it provides information both directly and indirectly. The evaporation gradient problem is solved by the updated direct-play action, letting the prototypical study earlier achieve improved [38]. The layer that contains all connections: A fully connected layer of brain material is one in which the influence of each layer is linked to each decision-making component in the layer below. The final few levels of most common AI models are fully linked layers that gather data from preceding layers to determine the production.

Output:
An optimistic, deleterious, or pneumonia accrue.

EXPERIMENTAL RESULTS

The fundamental motivation for the design and implementation of this framework is to facilitate the examination of picture data that conforms to preconceived notions of what should be there. Accordingly, structural constructs are means or strengths that demonstrate the structure, components, interfaces, modules, and data needed to implement the design principles. There is some sharing and cooperation between information gathering and the analysis of framework

methodologies [15] and framework structures. The projected profitability of the application serves as the foundation for evaluating capabilities and implementations. The salient qualities have considerably aided systems research. /A dominant structure can be built using the patient's relevant fundamental qualities. Finally, it fits our requirements. It also intends to establish a strong bond with the system's current users by utilizing unique needs.

ECNN Algorithm

The suggested and required enlargement of CNN to an all-encompassing ECNN(s) is thought to improve accuracy, execution, and time complexity. Tables 3 and 4 show the steps the suggested model followed to attain high accuracy and a low error rate.

Table 4: The ERNN approach's algorithm steps

Step 1: Import required libraries
Step 2: Pre-processing of the dataset
Step 3: Combined RNN with Extended Neurons
Step 4: Perform 10-folded cross-validation with 2 classes
Step 5: Import Keras deep learning library with all supported libraries
Step 6: Reset all parameters of ERNN
Step 7: Enhance the ERNN part and ablation of loss calculation function
Step 8: Enhancement of yield part of 10-folded with 2 classes
Step 9: Accumulate the ERNN parameters
Step 10: Adjusting the ERNN in the preparation of model
Step 11: Load the Skin Cancer disease infection image dataset
Step 12: Predicting the infection severity throbyssifying the dataset into 2 classes
Step 13: Outcome of the trained model and stop the model

ERNN Algorithm

The Skin Cancer dataset was submitted to ERNN following the processes outlined below.

As a result, the computations yield more precise answers and take less time to complete, stipulating the image's data in early anticipation.

DISCUSSION OF RESULTS

The outcomes of combining ERNN-ECNN, VGG-16, and GoogleNet on the Kaggle repository dataset for picture data detection are shown below.

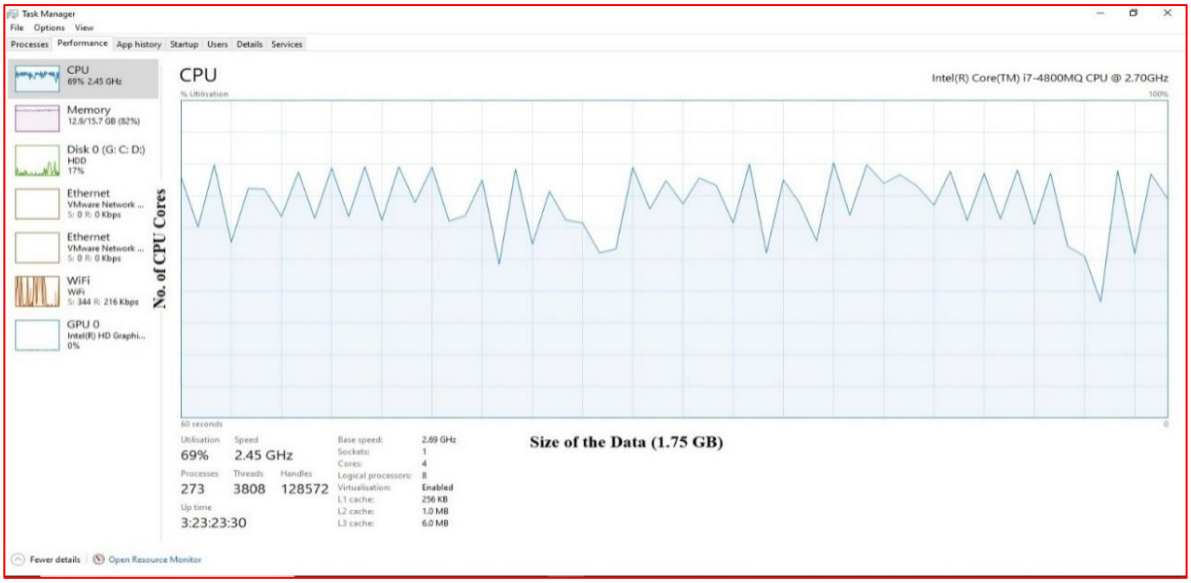

Fig. 4: Utilization of CPU resources in the Google, UCI, and Kaggle datasets for skin cancer CT-scan image data.

While running of experiment on skin cancer image dataset by using ECNN-ERNN deep learning techniques showing CPU utilization in the above figure 4.

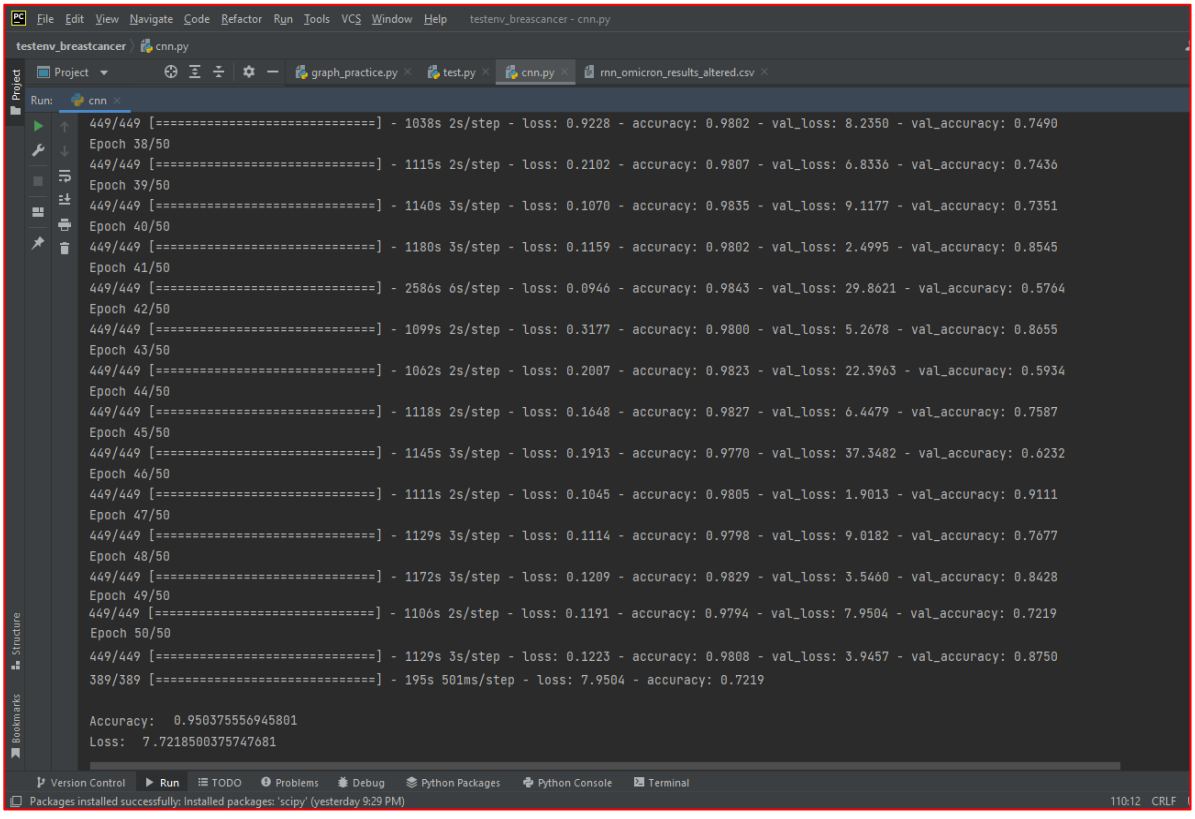

Fig. 5: ECNN stream execution on dataset preparation and testing

Figure 5 depicts the implementation flow across periods on the Skin Cancer dataset, which classifies events as negative or positive.

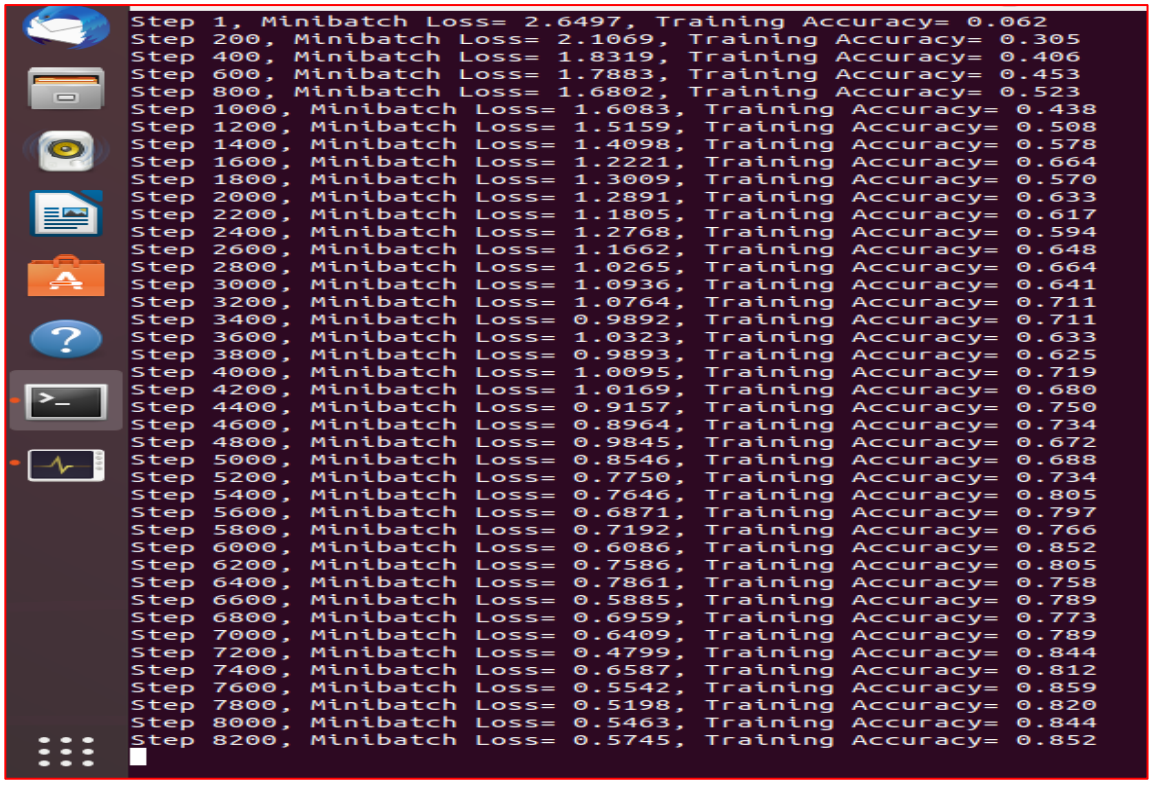

Fig.6: Applying the test dataset to run the ERNN flow

Figure 6 depicts the iterative execution flow of the ERNN method applied to the Skin Cancer dataset used by the projected model.

Evaluation Methods of Performance

To estimate and display the overall trial outcome, the most generally utilized factual approaches, such as precision, correctness, appraisal, F1-score, reaction, and fastidiousness, are applied. Since the limited number of cases in Study One, the quantifiable results are spoken with a 94.02% inevitability range. This is followed by lately published work, which also made use of a limited dataset [20, 23]. Skin cancer may be classed as true optimistic (Tp) or true undesirable (Tn) if persons are precisely examined in our dataset, or it may be classified as untrue optimistic (Fp) or untrue desirable (Fn) uncertainty misdiagnosed. The nuances listed below describe the assigned measurable measurements.

Accuracy:

It is the number of unique occurrences that have been identified in each instance that has been reported. When employing the associated methods, precision is not completely established:

$$Accuracy = \frac{\mathrm{Tp} + \mathrm{Tn}}{\mathrm{Fn} + \mathrm{Tp} + \mathrm{Fp} + \mathrm{Tn}}$$

Precision:

It is calculated as the fraction of obviously projected anticipated good outcomes.

$$Precision = \frac{Tp}{Fp + Tp}$$

Recall:
The number of important outcomes that are accurately distinguished by the calculation is referred to as recall.

$$Recall = \frac{Tp}{Fp + Tn}$$

Sensitivity:
The following measures of responsiveness can be used to determine whether a response is responsive:

$$Sensitivity = \frac{Tp}{Fn + Tp}$$

Specificity:
Using the formulas provided, it identifies the number of precisely perceived and determined certified negatives:

$$Specificity = \frac{Tn}{Fp + Tn}$$

F1-Score:
It is the perfect balance of audit and precision. The maximum likely F score is 1, which indicates exceptional audit accuracy.

$$F1 - Score = 2x\frac{Recall\ x\ Precision}{Recall + Precision}$$

AUC - Area under Curve:
The way to activate the models in more promising situations is discussed in the AUC. Using the associated function listed below, AUC can be resolved:

$$AUC = \frac{Xp\left(\frac{Xp+1}{2}\right) - \Sigma ri(Xp)}{Xn + Xp}$$

Metrics Evaluation
The proposed model used the going with systems to show and assess the effects of our suggested strategy on ERNN-ECNN strategies for the DL method. To investigate the chaos lattice, the terms "actual positive" (AP), "untrue positive" (UP), "actual negative" (AN), and "true negative" (UN) are initially defined in isolation. The no. of cases was appropriately expected due to OP. The following metrics are units of measurement for evaluation methods used to predict the projected model's quality, precision, callback, and F-measure.

Quality:
The Quality metrics are used to evaluate the value and performance of the research's services, procedures, and quality.

$$Quality = \frac{BP + VM}{BP + VP + BM + VM}$$

Preciseness:
A binary classifier's precision is a metric that determines whether all positive labels are accurate. A twofold classifier gives only two outcome values (for instance sure and negative).

$$Preciseness = \frac{BP}{VP + VM}$$

Callback:
An object that can act at a variety of training stages (like at the beginning or end of an era, before or after a single batch, etc.) referred to as a callback.

$$Callback = \frac{BP}{BP + VM}$$

F-Measure:
In binary classification statistical analysis, the F-score or F-measure of a test is used to measure its accuracy.

$$F - measure = \frac{2 * Preciseness * Callback}{Preciseness + Callback}$$

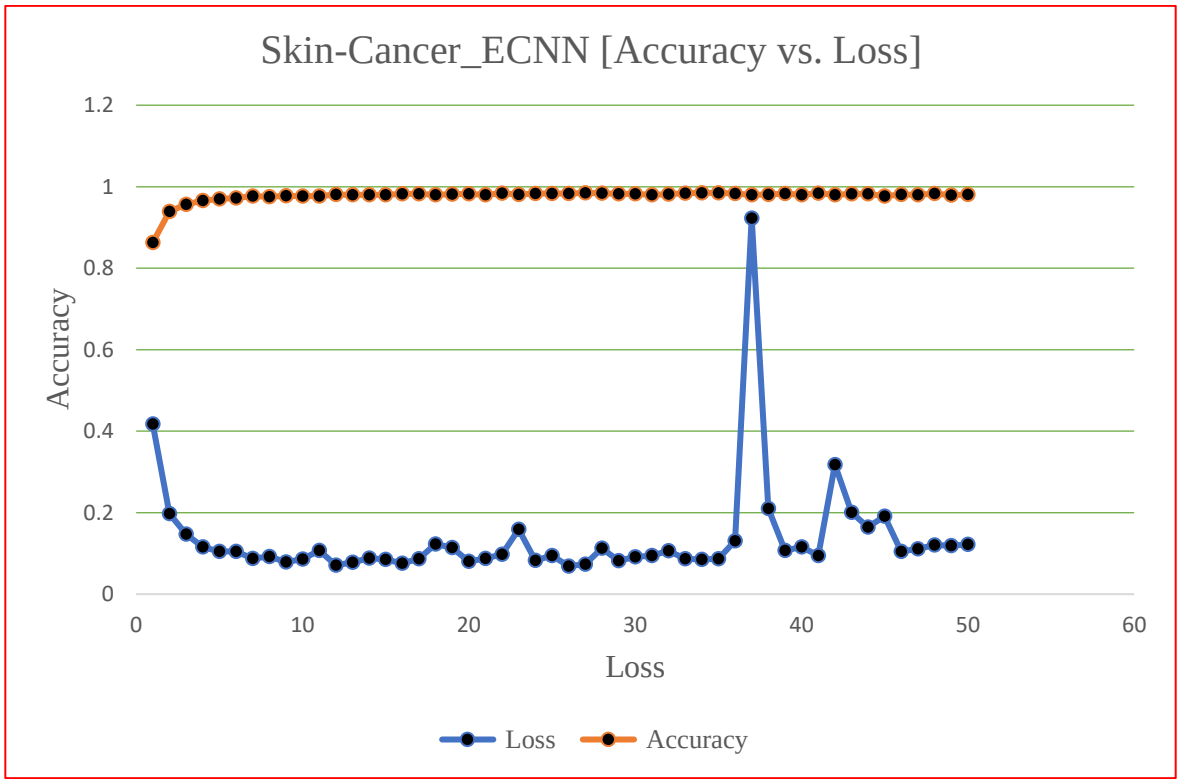

Fig.7: Accuracy versus loss in ECNN data for skin cancer

Figure 7 shows the time intervals that passed between Accuracy and Loss checks on the Skin Cancer dataset.

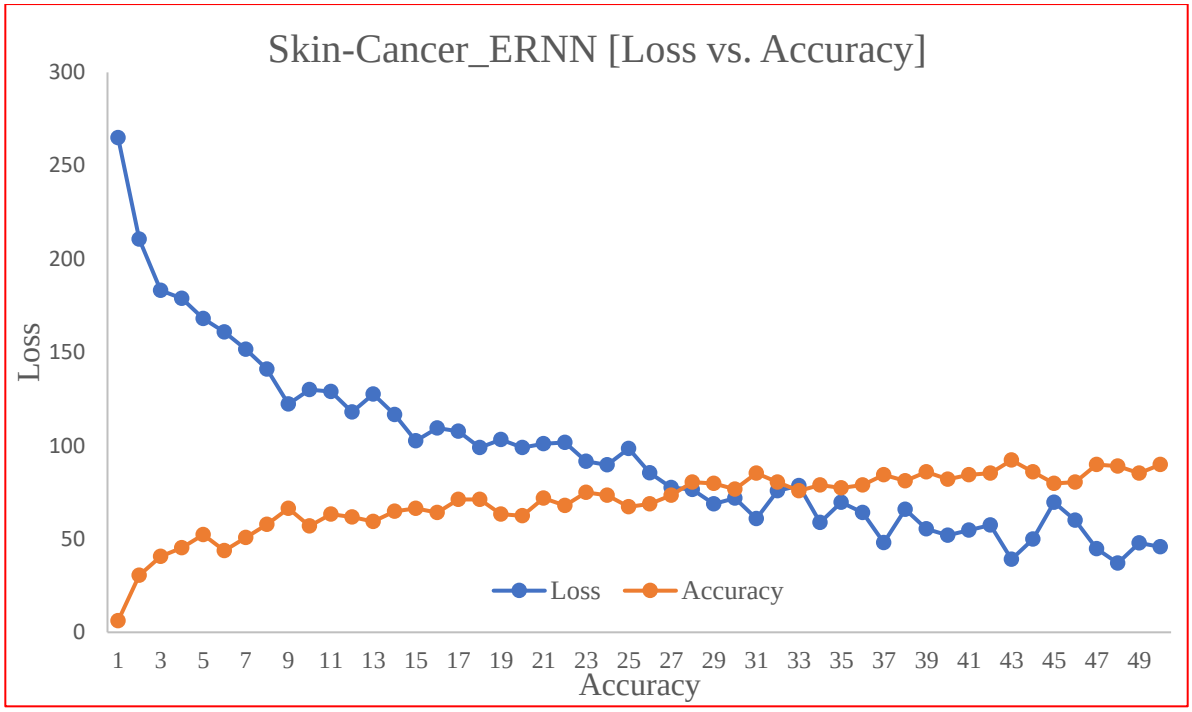

Fig. 8: Skin Malignant growth sickness ERNN information Exactness versus Misfortune

The execution epochs on the Skin Cancer testing and training dataset are depicted in Figure 8. These epochs are located between Accuracy and Loss.

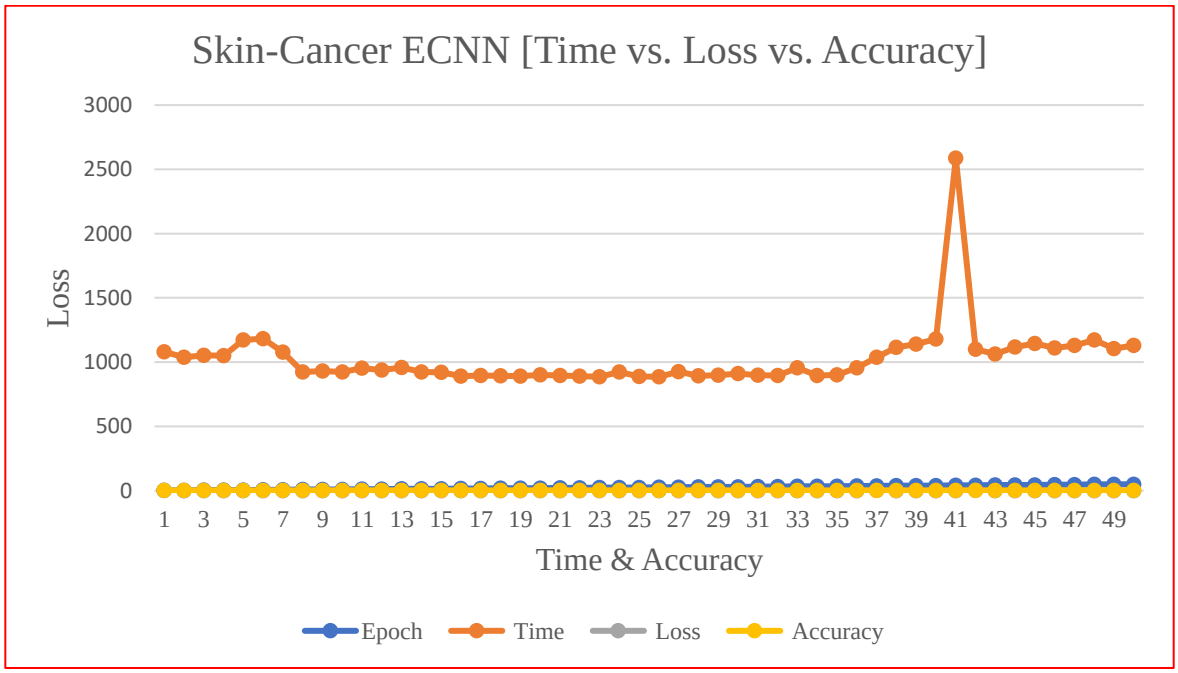

Fig. 9: Skin Malignant growth illness ECNN information Exactness versus Time

Figure 9 illustrates the execution epochs between Accuracy and Loss in relation to a time constraint to predict the proposed model's accuracy.

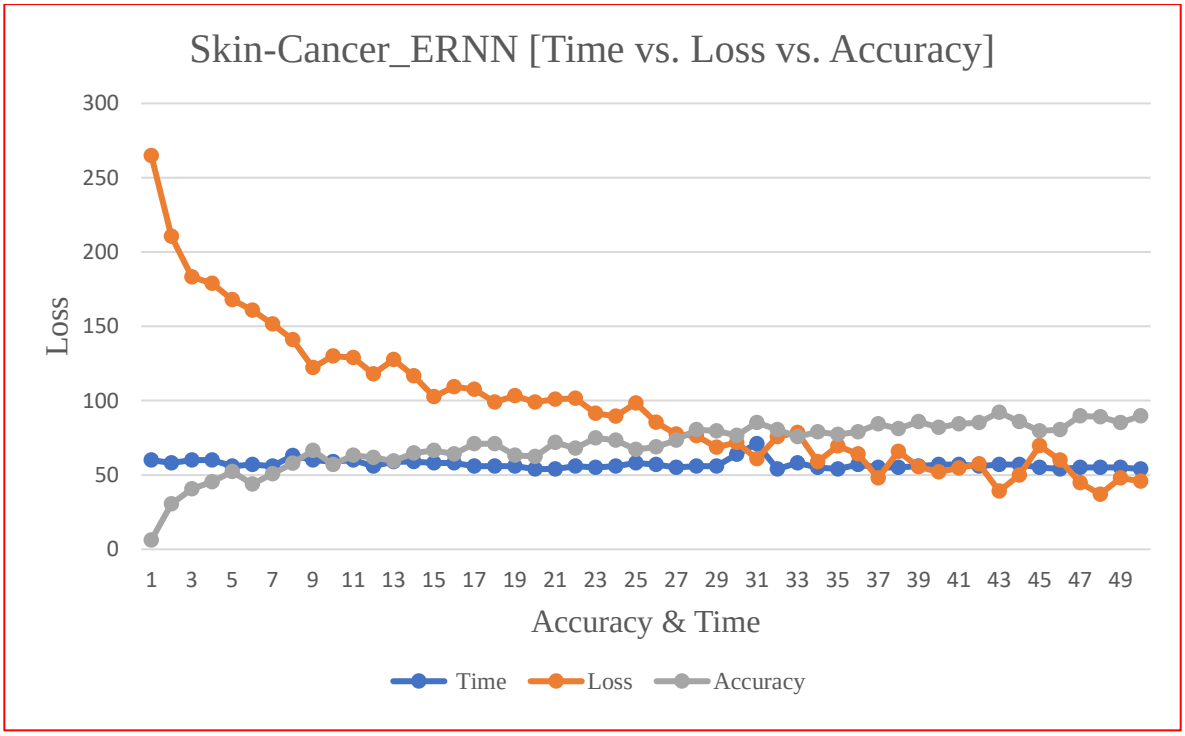

Fig. 10: Accuracy vs. Loss vs. Time: ERNN data on skin cancer

The above figure 10 explains the loss vs time vs accuracy parameters comparison on skin cancer image dataset by using deep learning techniques i.e., ECNN-ERNN approach.

The following table explains how the proposed techniques are compared to various parameters.

Comparison Table

The following table explains how the proposed techniques are compared to various parameters:

Table 5: Metrics compared using ECNN and ERNN techniques

S. No.	The parameter's name	ERNN	ECNN
1.	Execution time	1250 ms	1025ms
2.	Rate of error	0.56	0.14
3.	Loss Value	3.92	2.88
4.	Accuracy Value	0.79	0.97
5.	Dataset size	1.55 GB	1.55 GB
6.	Epochs	30	30
7.	Complexity time	$O(n^2)$	$O(n^2)$
8.	Accuracy	87.32%	94.02%

Based on multiple parameters, the comparison factors of the two methods are described in Table 5. The table comparison with accuracy is 87.32 of ERNN vs 94.02 of ECNN, time complexity is $O(n^2)$ of both proposed techniques of ERNN-ECNN approaches.

Time Complexity

Our method, it has been noted, necessitates more speculation than other systems currently in use. Utilizing a tensor dealing with the unit (TPU) and a reasonable planning unit (GPU) can significantly shorten this time. Additionally, the structure's presentation influences the amount

of time required to complete this task. At long last, structure execution is coordinated by framework programming and design gear.

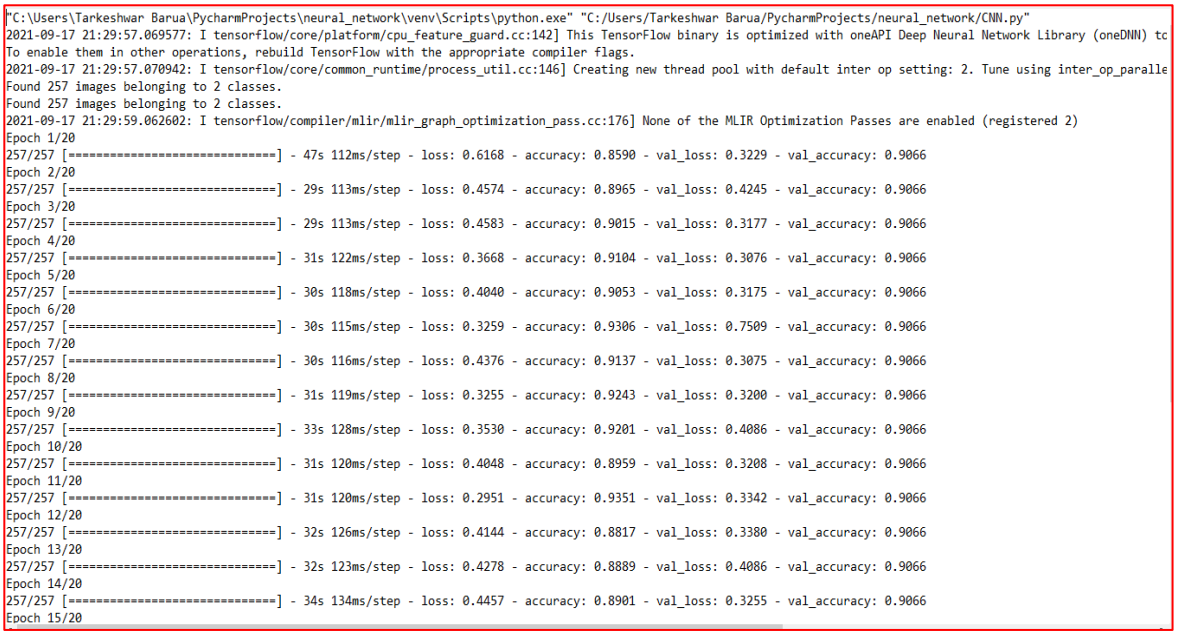

Fig 11: Makes sense of the Last result of the Skin Disease CT-examine picture informational collection from the Kaggle dataset.

The above figure 11 describes the number of epochs with accuracy is 87.32 of ERNN vs 94.02 of ECNN, time complexity is $O(n^2)$ of both proposed techniques of ERNN-ECNN approaches.

The hybrid ECNN-ERNN training and testing model has an accuracy of 95.35 percent and has room for improvement over several other models.

CONCLUSION

In this proposed research strategy, two classifications were employed, positive and negative, for the prediction of the error ratio and accuracy on 660 skin cancer patients' CT-scan images (hybrid ECNN-ERNN techniques). The proposed prototype employs ECNN-ERNN techniques of DL approaches to discover processes with improved reduced error and accuracy rates during the assessment, identification, and prediction procedures for skin cancer infection. In terms of parameters and measurements like accuracy, the new model performed better than the previous system (94.02%), error rate (0.13), val-loss (3.94), and val-accuracy (0.87). The number of epochs (30), the temporal complexity (O (n2)), and the execution time. In conclusion, we determined that the hybrid ECNN-ERNN model performed better in terms of precision during the analysis (87.32 %), error rate (0.56), loss value (3.92), accuracy value (0.79), and the size of the dataset on the disc used in this study when compared to the previous system (1.55 GB). The number of epochs (30), the time complexity (O(n2), and the duration (1025 milliseconds). The proposed model can be improved and used to anticipate and detect effective cases in a couple of seconds by including an IoT-based resilient mechanism. This approach has a promising future based on the framework that is employed and coupled to generate the required results.

REFERENCES

[1] ZaferCivelek et al.,"An Improved Deep CNN for an Early and Accurate Skin Cancer Detection, and Diagnosis System", International Journal of Engineering Research and Development, UluslararasıMühendislik, Araştırma ve GeliştirmeDergisi, UMAGD, (2022) 14(2), 721-734, Cilt/Volume:14 Sayı/Issue:2 Temmuz/July 2022, DOI: 10.29137/umagd.116295

[2] MdShahin Ali et al., "An enhanced technique of skin cancer classification using deep convolutional neural network with transfer learning models", Machine Learning with Applications 5 (2021) 100036, https://doi.org/10.1016/j.mlwa.2021.100036,

[3] S. Haggenmu¨ller et al. / European Journal of Cancer 156 (2021) 202e216, "Skin cancer classification via convolutional neural networks: systematic review of studies involving human experts", https://doi.org/10.1016/j.ejca.2021.06.0490959-8049/ª 2021 The Author(s). Published by Elsevier Ltd. This is an open access article under the CC BY-NC-ND license (http://creativecommons.org/licenses/by-nc-nd/4.0/).

[4] Boman, J., &Volminger, A. (2018). Evaluating a deep convolutional neural network for classification of skin cancer. In.

[5] Bray, F., Ferlay, J., Soerjomataram, I., Siegel, R. L., Torre, L. A., & Jemal, A. (2018). Global cancer statistics 2018: GLOBOCAN estimates of incidence and mortality worldwide for 36 cancers in 185 countries. CA: a cancer journal for clinicians, 68(6), 394-424.

[6] Brekhna, B., Mahmood, A., Zhou, Y., & Zhang, C. (2017). Robustness analysis of superpixel algorithms to image blur, additive Gaussian noise, and impulse noise. Journal of Electronic Imaging, 26(6), 061604.

[7] Daghrir, J., Tlig, L., Bouchouicha, M., & Sayadi, M. (2020). Melanoma skin cancer detection using deep learning and classical machine learning techniques: A hybrid approach. Paper presented at the 2020 5th international conference on advanced technologies for signal and image processing (ATSIP).

[8] Dorj, U.-O., Lee, K.-K., Choi, J.-Y., & Lee, M. (2018). The skin cancer classification using deep convolutional neural network. Multimedia Tools and Applications, 77(8), 9909-9924. Gedraite, E. S., &Hadad, M. (2011). Investigation on the effect of a Gaussian Blur in image filtering and segmentation. Paper presented at the Proceedings ELMAR-2011.

[9] Mahbod A, Schaefer C, Ellinger I, Ecker R, Pitiot A, Wang C. Fusing fine-tuned deep features for skin lesion classification. Comput Med Imaging Graph 2019; 71:19e29. Https://doi.org/10.1016/j.compmedimag.2018.10.007.

[10] Salerni G, Tera´n T, Puig S, Malvehy J, Zalaudek I, Argenziano G, et al. Meta-analysis of digital dermoscopy followup of melanocytic skin lesions: a study on behalf of the International Dermoscopy Society. J EurAcadDermatolVenereol 2013; 27:805e14.

[11] Vestergaard ME, Macaskill P, Holt PE, and Menzies SW. Dermoscopy compared with naked eye examination for the diagnosis of primary melanoma: a meta-analysis of studies performed in a clinical setting. Br J Dermatol2008; 159:669e76.

[12] Haenssle HA, Fink C, Schneiderbauer R, Toberer F, Buhl T, Blum A, et al. Man against machine: diagnostic performance of a deep learning convolutional neural network for dermoscopic melanoma recognition in comparison to 58 dermatologists. Ann Oncol2018; 29:1836e42.

[13] Lodha S, Saggar S, Celebi JT, Silvers DN. Discordance in the histopathologic diagnosis of difficult melanocytic neoplasms in the clinical setting. J CutanPathol2008; 35:349e52.

[14] Corona R, Mele A, Amini M, De Rosa G, Coppola G, Piccardi P, et al. Interobserver variability on the histopathologic diagnosis of cutaneous melanoma and other pigmented skin lesions. J ClinOncol1996; 14:1218e23.

[15] Tschandl P, Rosendahl C, Akay BN, Argenziano G, Blum A, Braun RP, et al. Expert-level diagnosis of nonpigmented skin cancer by combined convolutional neural networks. JAMA Dermatol2019; 155:58e65.

[16] Esteva A, Kuprel B, Novoa RA, Ko J, Swetter SM, Blau HM, et al. Dermatologist-level classification of skin cancer with deep neural networks. Nature 2017; 542:115e8.

[17] Nasr-Esfahani E, Samavi S, Karimi N, Soroushmehr SMR, Jafari MH, Ward K, et al. Melanoma detection by analysis of clinical images using convolutional neural network. In: 2016 38th annual international conference of the IEEE engineering in medicine and biology society. EMBC; 2016. p. 1373e6.

[18] Al-Masni, M. A., Al-Antari, M. A., Choi, M.-T., Han, S.-M., & Kim, T.-S. (2018). Skin lesion segmentation in dermoscopy images via deep full resolution convolutional networks. Computer Methods and Programs in Biomedicine, 162, 221–231.

[19] Alfed, N., Khelifi, F., Bouridane, A., &Seker, H. (2015). Pigment network-based skin cancer detection. In 2015 37th annual international conference of the IEEE engineering in medicine and biology society (EMBC) (pp. 7214–7217). IEEE.

[20] Aljanabi, M., Özok, Y. E., Rahebi, J., & Abdullah, A. S. (2018). Skin lesion segmentation method for dermoscopy images using artificial bee colony algorithm. Symmetry, 10(8), 347. Biessmann, F., Salinas, D., Schelter, S., Schmidt, P., & Lange, D. (2018). "Deep" learning for missing value imputation in tables with non-numerical data. In Proceedings of the 27th ACM international conference on information and knowledge management (pp. 2017–2025).

[21] Canadian Cancer Society's Advisory Committee on Cancer Statistics (2014). Canadian cancer statistics 2014 - special topic: Skin cancers. Retrieved from https://www. Cancer.ca/statistics. (Accessed 30 December 2020).

[22] Cancer Council Australia (2018). Understanding skin cancer - a guide for people with cancer, their families, and friends. Retrieved from https://www.cancer.org. au/about-cancer/types-of-cancer/skin-cancer.html. (Accessed 30 December 2020).

[23] Ravikumar CV, Kala Praveen Bagadi, Design of MC-CDMA receiver using RBF network to mitigate MAI and nonlinear distortion, Neural Computing and Applications, Vol.31, Issue 2, 2019.

[24] Ravikumar CV, Kala Praveen Bagadi, MC-CDMA receiver design using recurrent neural network for eliminating MAI and non-linear distortion, International Journal of Communication Systems (IJCS), Vol.10 , Issue 16, 2017.

[25] K. Bagadi et al., "Detection of Signals in MC–CDMA Using a Novel Iterative Block Decision Feedback Equalizer," in IEEE Access, vol. 10, pp. 105674-105684, 2022, doi: 10.1109/ACCESS.2022.3211392.

[26] Asadi Srinivasulu, Rajesh, A., Olutayo Oyeyemi Oyerinde, "Performance and Improvement Analysis of the Underwater WSN Using a Diverse Routing Protocol Approach", Journal of Computer Networks and Communications, vol. 2022, Article ID 9418392, 19 pages, 2022. https://doi.org/10.1155/2022/9418392.

[27] K, S.; CV, R.; A, R.; Pau, G. Underwater Wireless Sensor Network Performance Analysis Using Diverse Routing Protocols. J. Sens. Actuator Netw. 2022, 11, 64. https://doi.org/10.3390/jsan11040064.

[28] Sathish, K.; Anbazhagan, R.; Venkata, R.C.; Arena, F.; Pau, G. Investigation and Numerical Simulation of the Acoustic Target Strength of the Underwater Submarine Vehicle. *Inventions* 2022, *7*, 111. https://doi.org/10.3390/inventions7040111.

[29] Xiangjie Kong, Zhiqiang Huang, Guojiang Shen, Hang Lin, Mingjie Lv. "Urban Overtourism Detection Based on Graph Temporal Convolutional Networks" IEEE Transactions on Computational Social Systems 2022. DOI: 10.1109/TCSS.2022.3226177.

[30] Xiangjie Kong, Yuhan Wu, Hui Wang, and Feng Xia. "Edge Computing for Internet of Everything: A Survey." IEEE Internet of Things Journal 9, no. (23), pp.23472–23485, 2022.

[31] Xiangjie Kong, Qiao Chen, MingliangHou, Azizur Rahim, Kai Ma, and Feng Xia. "RMGen: A Tri-Layer Vehicular Trajectory Data Generation Model Exploring Urban Region Division and Mobility Pattern." IEEE Transactions on Vehicular Technology 71, no. (9), pp.9225–9238, 2022.

[32] Xiangjie Kong, Ning Li, Chenwei Zhang, Guojiang Shen, Zhaolong Ning, and Tie Qiu. "Multi-Feature Representation based COVID-19 Risk Stage Evaluation with Transfer Learning." IEEE Transactions on Network Science and Engineering 9, no. (3), pp.1359–1375, 2022.

[33] Xiangjie Kong, Kailai Wang, Shupeng Wang, Xiaojie Wang, Xin Jiang, Yi Guo, Guojiang Shen, Xin Chen, and Qichao Ni, Real-time Mask Identification for COVID-19: An Edge Computing-based Deep Learning Framework. IEEE Internet of Things Journal8, no. (21), pp.15929-15938, 2021.

[34] Xiangjie Kong, Bing Zhu, Guojiang Shen, TewabechekoleWorkneh, Zhanhao Ji, Yang Chen, and Zhi Liu. "Spatial-Temporal-Cost Combination based Taxi Driving Fraud Detection for Collaborative Internet of Vehicles." IEEE Transactions on Industrial Informatics 18, no. (5), pp.3426–3436, 2022.

[35] Xiangjie Kong, GaohuiDuan, MingliangHou, Guojiang Shen, Hui Wang, Xiaoran Yan, and Mario Collotta, Deep Reinforcement Learning based Energy Efficient Edge Computing for Internet of Vehicles. IEEE Transactions on Industrial Informatics18, no. (9), pp.6308–6316, 2022.

[36] Xiangjie Kong, Kailai Wang, MingliangHou, XinyuHao, Guojiang Shen, Xin Chen, Feng Xia, A Federated Learning-based License Plate Recognition Scheme for 5G-enabled Internet of Vehicles, IEEE Transactions on Industrial Informatics 17, no. (12), pp.8523–8530, 2021.

[37] Xiangjie Kong, HaoranGAO, Guojiang Shen, GaohuiDuan, Sajal K. Das, FedVCP: A Federated Learning based Cooperative Positioning Scheme for Social Internet of Vehicles, IEEE Transactions on Computational Social Systems9, no. (1), pp.197–206, 2022

[38] Guojiang Shen, Xiao Han, KwaiSang Chin, and Xiangjie Kong. "An Attention-Based Digraph Convolution Network Enabled Framework for Congestion Recognition in Three-Dimensional Road Networks." IEEE Transactions on Intelligent Transportation Systems23, no. (9), pp.14413–14426, 2022.

Journal of Research in Engineering and Computer Sciences
August 2023, Vol. 1, No. 3, pp. 33-40

Novel Electricity Distribution Pillar Development

Arinze W. Nwosu[1], Uche P. Chukwu[2] and Michael C. Amonye[3]

1. Department of Electrical/Electronic Engineering, Chukwuemeka Odumegwu Ojukwu University, Uli Campus, Anambra State
2. National Board for Technology Incubation (NBTI), Federal Secretariat, Phase 2, Block C, Garki, Abuja
3. Products and Processes Ltd, 42 Stadium Quarters, Kwali FCT, Abuja

Abstract:
Transmission and distribution of electrical energy is one of the most critical aspects of electrical power supply. Conventional distribution or feeder pillars do not allow physical identification of line/lines required for upgrade to unload it before it results to hazard and catastrophic damage. It is important that, both incoming phases and outgoing lines are secured to avoid escalating damages by isolating the faults before failure or any damage occurs. Novel Electricity Distribution Pillar is designed to improve safety of lives and properties by ensuring quality power is being provided during distribution. The innovation enables independent control of outgoing lines wherefore faults can be easily isolated and reported promptly without interrupting other lines. The equipment ensures that incoming phases and outgoing lines are adequately fused which serves as the secondary protection system. The track records of power supplied are first taken and measured at the incoming phase fuse link via a voltmeter and current transformers connected to each phase independently. The introduction of Novel Electricity Distribution Pillar proposes to enhance operator safety, reduction in electrical hazards leading to smooth maintenance operations and better electricity supply in Nigeria.

Keywords: Electricity, Distribution, Hazard, Feeder, Pillar, Safety

INTRODUCTION

Continuous enhancement of human and industrial activities engendering corresponding increase in the use of power both domestically and in industries, prompts the need to adequately protect our homes, industries and every other electrical appliance using electricity. After the generation and distribution of electricity, it cannot be assumed that the consumers will efficiently manage the power ensuring powering off gadgets and devices when not in use. Inefficient management can lead to losses and may constitute serious problems to the load users as well as the operators. In order to have adequate control and full management of power supplied without shutting down the generation or transmission station which will affect the entire user for the purpose of maintenance at the end user point, a feeder pillar station is set up to either isolate a fault or a line for any operation as the case may be. A distribution pillar (also known as a power box, feeder pillar, or feeder pillar box) is a cabinet which is used to house electrical distribution equipment, consisting of a panel which embodies all other sub-units of the feeder pillar, bus-bars in which are connected the incoming and outgoing lines, an ammeter which records the voltage across the bus-bars, the fuse holders holds the fuses, high-rupturing-capacity fuses for making contact and for protection purposes (Azuatalam *et al.*, 2014). Feeder pillars act as a central circuit in control and distribution of electricity to outgoing circuits downstream to the feeder pillar. It is designed to provide each circuit protection, along with the capacity to be easily controlled. However, feeder pillars over the years have received significant attention to be investigated, on how to improve its protection abilities to safeguard lives and properties.

The common failure experienced by electrical appliances is associated to phase failure which could be caused by either unbalanced voltage, single phasing or phase loss, overloads, power outage, overvoltage, under voltage, or phase reversal. Similarly, since phase failure cannot be avoided in our everyday electricity consumption, it is paramount to note that phase failure detector is a very vital protective device that must be taken seriously (Ezema, 2012). Phase failure detectors enable operators to fix the faults and restore power in due time. The fixing of phase failures is very delicate as most fatal accidents that lead to loss of lives and property such as flashover and arc flash are experienced during the work. Plates 1 and 2 depicts the conventional feeder pillars.

Plate 1. 4-Way LT Feeder Pillar

Plate 2. 6-Way LT Feeder Pillar

These types of feeder pillars do not have an incoming switch nor fuse. Rather, the outgoing lines have fuses, while, the incoming phases are connected directly to the phase bus bars, thus, the operator do not have utmost control over the circuit. These conventional feeder pillars cannot be used to effectively allocate and distribute electrical energy without putting the operators' lives at risk and must have to rely on the substation to turn off the incoming lines before work can be done with limited risk, thus, affecting the consumer until power is restored after maintenance. About 80% of electrically related accidents and fatalities involving "Qualified Workers" are caused by arc flash / arc blast. Similarly, the feed pillars shown in Plate 3 and 4 below, have a slight difference from the feeder pillars described in Plate 1 and 2.

Plate 3. 4-Way LT Feeder Pillar with Circuit Breaker

Plate 4. 4-Way LT Feeder Pillar with Manual Switchgear

These types of feeder pillars come with incoming circuit breakers/switchgears, but, turning on and off requires human involvement which can result to fatal accidents. The feeder pillar shown in Plate 5 has an added advantage with additional fuse for the incoming lines, but will still require human presence to disengage fuses or turn off switches for maintenance. Although, when switches are turned off, all the lines are also disengaged together with the faulty line.

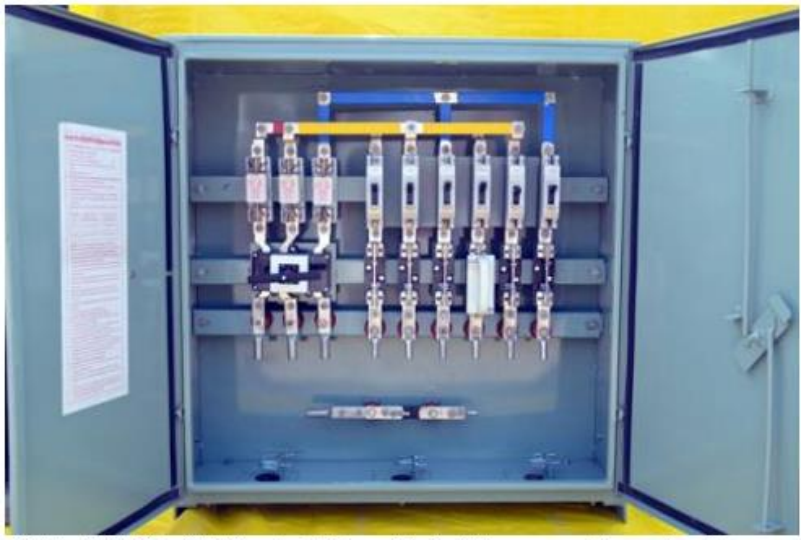

Plate 5: 2-Way LT Feeder Pillar with Switchgear and incoming fuse

The conventional distribution or feeder pillars do not serve well as long as effective energy distribution, real-time and actual fault detection, and safety are the priority. The conventional feeder pillars do not have the ability to monitor the power supplied and power evacuated. Likewise, the safety of the electrical appliances solely depends on the breakers and fuses which in some cases tend to fail in operation, thus, endangering the stations and the end users. In addition, a vast majority of electrical incidents occur because people are working on or near equipment that is either thought to be dead but is still live or by those working on equipment that is known to be live but they do not have the adequate training or are not using adequate protection equipment.

Furthermore, the conventional feeder pillars do not have tracks and records of load buildup over time. Unfortunately, excess load on the lines is usually identified when the overloaded fuse cuts/melts, thus, increases the maintenance cost of the system. Similarly, a lot of fuses are damaged due to human factor when allocating energy. Likewise, the fuse base develops mechanical faults due to frequent pulling and inserting of fuses over time, which makes the fuse base loose grip of the fuse link. This leads to partial contact and eventually, can lead to fire outbreak when not addressed immediately, whereby, the operator may possibly experience arc flash or flashover. To curb all these anomalies, secure installations and reduce damage emanating from the employment of conventional electricity distribution pillars, this novel equipment is built to identify and isolate faults promptly without interrupting other lines. The equipment ensures that incoming phases and outgoing lines are adequately fused which serves as the secondary protection system. The track records of power supplied are first taken and measured at the incoming phase fuse link via a voltmeter and current transformers connected to each phase independently.

MATERIALS AND METHODS

The isometric drawing of the Novel Electricity Distribution Pillar is shown in Figure 1. It depicts the outside view of the device when the entire components are enclosed. The orthographic view of Pillar is shown in Figure 2 while the exploded view is shown in Figure 3. The instrument has a Control Compartment (1) which houses all the monitoring and actuating components, and the Switching Compartment (5) which houses all transmission connections and switching devices. In addition, as ventilation is required to evacuate warm air, two Louvers (4) are provided for each compartment, both located at the lower sides of the compartments. While behind the Top Cover (6), addition Louver is made for warm air escape route for both compartments. The maximum size the device occupies is (1453 X 330 X 1135 mm) (L x B x H). It also shows the positioning of the cable input via the Cable Glands (31), which are located at the top right and left bottom of the Switching Compartment (5).

Novel Electricity Distribution Pillar comprises of the Control Compartment (1), Front-Lower Cover (2), Louvers (4), Switching Compartment (5), Top Cover (6), Cover 1 (7), Cover 2 (8), Seal 1 (9), Seal 2 (10), Switchgear (11), Current Transformer (12), HRC Fuse Link (NT – 400) (13), HRC Fuse Link (NT – 800) (14), Keylock (15), SP Fuse Base (16), Phase Bus bar Red (17), Phase Bus bar Yellow (18), Phase Bus bar Blue (19), Phase Bus bar 400A – Blue (20), Phase Bus bar 400A – Red (21), Phase Bus bar 400A – Yellow (22), 6A Miniarture Circuit Breaker (23), 10A Relay (24), 12V DC Adapter (25), Analog Meter (26), Digital Meter (27), Load Indication (28), Power Indicator (29), Rowtina Smart Module (30), Cable Gland (31), Bus bar Insulator (32), Neutral Bus bar (33) and Line Current Transformer (35).

The 3 Phases power supply and Neutral cables are passed through 4 Cable Glands (31) under the Switching Compartment (5), each in a single hole. The phases are connected individually to the lower end of the 3-SP Fuse Base (16) in which HRC Fuse Link (NT – 800) (14) are mounted on. The HRC Fuse Link (NT – 800) (14) are designed to cut/melt when Load current is beyond 800A. Each of the 3-SP Fuse Base have one Current Transformer (12) right around the SP Fuse Base (16) and Phase Bus bars (17, 18 and 19) to constantly measure the amount of accumulative current drawn on each of the Phase Bus bars (17, 18 and 19). Depending on the current demands, more than two lines can be drawn from each of the Phase Bus bar (17, 18 and 19). Two lines of each of the Phase Bus bar 400A (20, 21 and 22) were drawn to each of the Phase Bus bar (17, 18 and 19) and connected to two separate 400A Switchgear (11) as shown in Figure 4, thus, splitting the Load current into two. Also, each 400A Switchgear (11) operates individually as each can be maintained which out interrupting another. Similarly, at the other end of the two 400A Switchgear (11), the SP Fuse Base (16) are also connected to each of the terminals. Whereas, the other end of the SP Fuse Base (16) serves as load connection points, where each line has a Line Current Transformer (35), which also measures the current consumed by each line independently. Simultaneously, current measured is alongside with the voltage supplied on a particular phase independent of the other phase. Although, the general voltage measured for each phase and power supplied to the control systems are drawn from the phase connection points of the SP Fuse Base (16) before fused with the HRC Fuse Link (NT – 800). This will enable the control systems powered for communication and control even when the fuses are out. However, on the Line Phases, voltage is measured right after fused, at the SP Fuse Base (16) terminal for load connection so that zero voltage will signal fault to the model for that particular line.

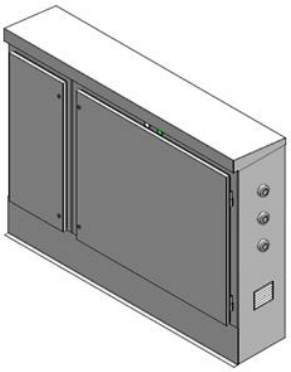

Figure 1: Isometric View of the Novel Electricity Distribution Pillar

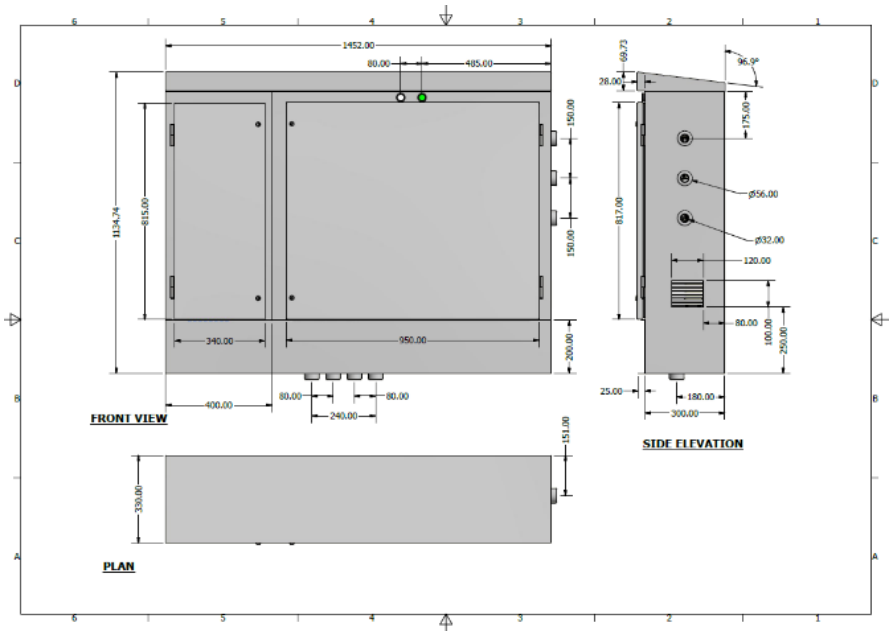

Figure 2: Orthographic View of the Novel Electricity Distribution Pill

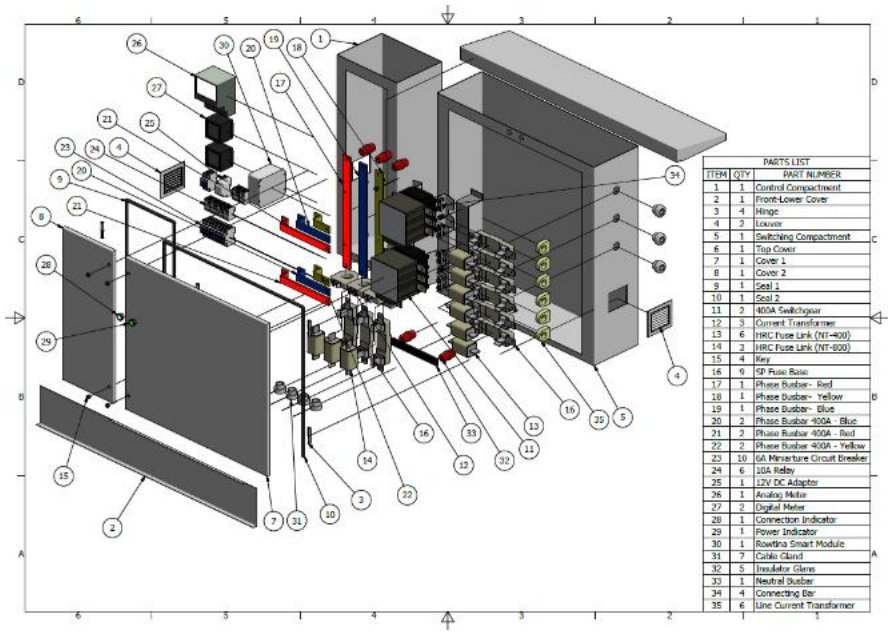

ITEM	QTY	PART NUMBER
1	1	Control Compactment
2	1	Front-Lower Cover
3	4	Hinge
4	2	Louver
5	1	Switching Compactment
6	1	Top Cover
7	1	Cover 1
8	1	Cover 2
9	1	Seal 1
10	1	Seal 2
11	2	400A Switchgear
12	3	Current Transformer
13	6	HRC Fuse Link (NT-400)
14	3	HRC Fuse Link (NT-800)
15	4	Key
16	9	SP Fuse Base
17	1	Phase Busbar- Red
18	1	Phase Busbar- Yellow
19	1	Phase Busbar- Blue
20	2	Phase Busbar 400A - Blue
21	2	Phase Busbar 400A - Red
22	2	Phase Busbar 400A - Yellow
23	10	6A Miniature Circuit Breaker
24	6	10A Relay
25	1	12V DC Adapter
26	1	Analog Meter
27	2	Digital Meter
28	1	Connection Indicator
29	1	Power Indicator
30	1	Rowtina Smart Module
31	7	Cable Gland
32	5	Insulator Clamp
33	1	Neutral Busbar
34	4	Connecting Bar
35	6	Line Current Transformer

Figure 3: Exploded View of the Novel Electricity Distribution Pillar

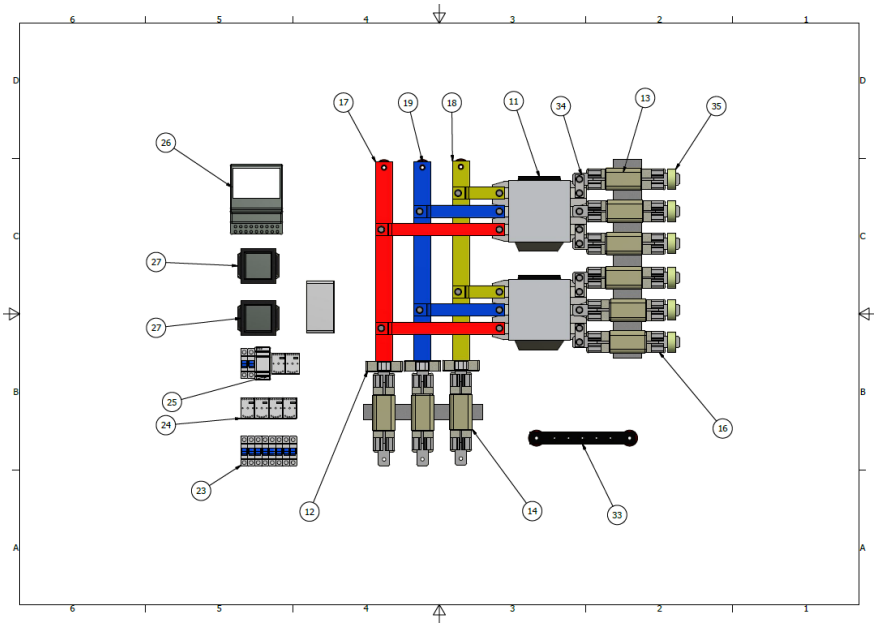

Figure 4: Front View of the Control Systems and Switching Gears

An Analog Meter (26) is used to calculate the total energy consumed by the station using the Current Transformers (12) mounted to each Phase Bus bar (17, 18 and 19). Whereas, the two Digital Meters (27) measure the lines voltage and current simultaneous. Each line voltage measured must pass through a 6A Miniature Circuit Breaker (23). Hence, all data computed by the Analog Meter (26) and the Digital Meters (27) are harvested by the Rowtina Smart Module (30) for further analysis. The Rowtina Smart Module is powered by a 12V DC Adapter (25) having a 3-Phase power supply system. Whereby, the power supplied to the Rowtina Smart Module (30) will not solely depend on a single phase, thus, when a phase is out, monitoring and communication will continue so are faults will be corded and reported promptly. Moreover, when the Rowtina Smart Module (30) is connected to the internet, the Communication Indicator (28) light comes on, while and immediately the internet service is no longer available, Communication Indicator (28) will go off. Similarly, when power is available in the Rowtina Switchgear Feeder Pillar, the Power Indicator (29) also comes on.

Meanwhile, the two 400A Switchgear (11) are actuated by the Rowtina Smart Module (30), through 10A Relays (24). Each 400A Switchgear (11) is connect to three 10A Relays (24), receiving power from each of the Phases. However, only one phase is used at a time to actuate the 400A Switchgear, which will be substituted by the module when the phase is out due to fuse failure. Although, 400A Switchgears are actuated independently, thus, ensuring that power is supplied to other lines before the fault is be rectified. Furthermore, Rowtina Smart Module (30) is designed to store and safe data. Whereas, data computed in the module can be sent to mobile phones via SMS to a configured mobile number, or to a web server database for visual representation. The module when powered, it takes 10 seconds to update it data from the EEPROM and synchronizes it current configuration from the server via ESP32 WiFi Module that is installed in it for web communication. Thus, enable the continuation of scheduled switching control and energy allocation. Similarly, a secondary backup timer powered by the RTC battery is added to the Rowtina Smart Module (30) mainboard which preserves the system clock and hardware state, in order to maintain scheduling even when online time isn't available immediately powered is restored to the grid.

In addition, the Rowtina Smart Module has a "Bypass mode", which allows the automatic control to be override. The Bypass mode is activated either when the internet service isn't available or when the Rowtina Smart Module (30) is faulty. However, the last schedule switching is maintained and returned to default at the end of the scheduled time while internet service is still not available for updates, whereas, when the Rowtina Smart Module (30) is faulty, the Bypass is manually set to put the system in constant default mode.

RESULTS

Novel Electricity Distribution Pillar is presented in Plate 6 and Plate 7. Plate 6 depicts the inside arrangement of the Feeder Pillar while Plate 7 is the picture when closed. The major components namely: an analog meter, digital voltmeter and ammeter, current transformers, 6A miniature circuit breakers, 12V DC adapter, Rowtina Smart Module, 6A relays, 400A contactors, control compartment and switching compartment are here arranged and installed into a box as Novel Electricity Distribution Pillar. It allocates energy to lines independently, sends and receives notifications both as SMS and/or on website, detect faults, report and isolate the faulty line until the fault is cleared before restoring the line's connections, as well as enable the control through SMS or website signals.

Plate 6: The inside of Novel Electricity Distribution Pillar (open)

Plate 7: Novel Electricity Distribution Pillar (closed).

CONCLUSION

The Department of Electrical/Electronic Engineering, Chukwuemeka Odumegwu Ojukwu University, Anambra State, Nigeria in collaboration with the National Board for Technology Incubation (NBTI), Abuja, developed a novel Electricity Distribution Pillar from locally available materials. The device allocates energy and schedules switching time without constant removing and inserting of fuse link through a 400A switching device used as switchgear. This cuts out damaging of fuse link and fuse base and possibly arc flash / arc blast and flash over. In the case of emergency or on request, the system communicates with the operator by sending data through a Rowtina Smart Module to either a cell phone as SMS or web server via the internet in an HTTP format without the operator reaching the site for instant investigation. The introduction of Novel Electricity Distribution Pillar proposes to enhance operator safety and reduction in electrical hazards leading to smooth maintenance operations and better electricity supply in Nigeria.

REFERENCES

[1]. D. T. Azuatalam, U. H. Diala, U. C. Iwuchukwu, C. K. Joe-Uzuegbu, F. C. Morah and E. I. Ayalogu. Design, Construction and Simulation of a Circuit Breaker Based Feeder Pillar with over current And Earth-Fault Protection Cum Digitalized Voltmeter. Int. J. of Eng. and Inno. Tech. (IJEIT) Volume 4, Issue 2, pp. 148-153. August, 2014

[2]. L. S.Ezema, B. U. Peter and O. O. Harris O. O. Phase Failure Detector and their Significance in Power System Engineering. Acad. Res. Int. Vol. 3, No. 2, pp. 218-223, September, 2012.

Journal of Research in Engineering and Computer Sciences
August 2023, Vol. 1, No. 3, pp. 41-42

Ground State Electron Energies in sp_3 Hybridized Si and C Atoms in 4H-SiC Calculated from Ionization Energies

Ravi Kumar Chanana

1. Self-Employed Independent Researcher, Gr. Noida-201310, India

Abstract:
In this research article, the ionization electron energies of sp3 hybridized Si and C atoms in 4H-SiC are calculated. The Si and C atoms are bonded tetrahedrally in 4H-SiC. The potential energy difference is found to be 0.13 eV from the ionization energies. The minimum number of Si-C bilayers are further calculated as 25 in 4H-SiC to give a theoretical bandgap of the bulk material as 3.25 eV, very close to the value of 3.26 eV calculated by applying the density functional theory.

Keywords: Bandgaps, Ionization, 4H-SiC, Composite semiconductor materials.

INTRODUCTION

4H-SiC semiconductor is technologically important semiconductor for high voltage power electronics applications with the advent of a power MOSFET such as a 650V MOSFET manufactured by the company called Infineon. This paper studies some relevant basic science of the 4H-SiC semiconductor material. Two recent articles by the author reports the minimum number of Si-C bi-layers needed in SiC semiconductor material so that the semiconductor exhibits the bulk semiconductor bandgap. The difference in the two papers is that the energy difference between the interacting electrons in the Si and C atoms of SiC are reported different. In one paper it is reported as 0.14 eV and in the other paper it is reported as 0.13 eV [1-2]. It needs to be stated that 0.13 eV is the correct energy difference and the calculation is shown in the present article starting from the ionization energy formula.

THEORY

SiC polytypes have different stacking sequence of the tetrahedrally bonded Si-C bilayers such as 3C-SiC has the sequence of ABCABC... of three positions with respect to the lattice denoted as A, B, and C. Similarly, 2H-SiC has the sequence ABAB..., 4H-SiC has the sequence ABCBABCB...., with 4 layers repeated, and 6H-SiC has the sequence ABCACBABCACB..., with 6 layers repeated. The ground state energy levels of the interacting electrons of a Si and C atom in SiC has shown a difference of 0.13 eV in energy [3]. This energy difference can be calculated from the ionization energies of electrons in Si and C atoms forming tetrahedral bonds with the sp^3 hybridized bonds in both Si and C. The formula for the ionization energy of an atom is given as:

$$E_n = -13.6 \times n^2/Z^2 \text{ in eV/atom,}$$

where n is the shell number in the atomic configuration and Z is the atomic number of the atom.

RESULTS AND DISCUSSIONS

The ionization energies for 4 electrons and one electron in Si and C atoms is calculated utilizing the formula for ionization energy presented in the theory section. The results are tabulated below

Table 1. Ionization energies of electrons in Si and C atoms

Elements	Atomic Number, Z	Shell Number, n	Ionization Energies of 4 electrons in eV	Ionization Energies of 1 electron in eV
Si	14	3	- 0.6244	- 0.1561
C	6	2	- 1.5111	- 0.3777

Furthermore, the p-orbital after sp^3 hybridization in C atom changes the angle from 90^o to 109.47^o. The change in angle is 19.47^o. Therefore, the ionization energy of the electron of the sp^3 orbital increases by -0.3777/Cos (19.47^o) =- 0.40 eV as the potential energy of one electron of the C atom at the corner of the unit cell. To form the sp^3 tetrahedral bond in 4H-SiC for example, the orbital lies along the body diagonal of the unit cell of size 2, from the centre having Si atom to the corner having C atom. The p-orbital after hybridization reduces in size causing the Coulombic force between the two interacting electrons to increase. The work done is force times the distance. Therefore, the energy of the electron therefore increases by the factor of the body diagonal of $\sqrt{3}$. Assuming a bond with Si at the centre and the C at the corner makes the energy of the Si sp^3 electron as -0.1561 x $\sqrt{3}$ = -0.270 eV as the potential energy of one electron of the Si atom at the centre. The difference in the sp^3 electron energies becomes -0.27- (-0.40) = 0.13 eV [3].

It can be calculated that the minimum number of Si-C bilayers with this energy difference of 0.13 eV will be 25 for the 4H-SiC to give the theoretical bandgap of 0.13 x 25 = 3.25 eV [1-2]. The study utilizing the density functional theory reports a value of 3.26 eV as the bandgap of 4H-SiC [4]. The experimental bandgap of 4H-SiC is reported as 3.23 eV [5].

CONCLUSION

The ionization energies as the potential energy of one electron each in the Si and C atom of tetrahedrally bonded 4H-SiC are -0.27 eV and -0.40 eV respectively after sp^3 hybridization of both the atoms and forming the tetrahedral bond. The minimum number of Si-C bilayers in 4H-SiC semiconductor are calculated to be 25, to give a theoretical bandgap of 3.25 eV. The method could be applied to other composite semiconductor materials, and could form a new method to find the bandgap of a semiconductor.

REFERENCES

[1]. R.K. Chanana, *Minimum number of Si-C bilayers needed in polytypes of SiC semiconductor to exhibit bandgaps of bulk materials*, TECS, U.K., 2023. 11(4), p. 19-20.

[2]. R.K. Chanana, *Minimum number of Si-C bilayers needed in polytypes of SiC semiconductor to exhibit bandgaps of bulk materials*, IOSR-Journal of Appl. Phys., 2023. 15(4), p. 4-5.

[3]. J. Borysiuk, J. Soltys, R. Bozek, J. Piechota, S. Krukowski, W. Strupinski, J.M. Baranowski, R. Stepniewski, *Role of structure of C-terminated 4H-SiC (ooo-1) surface in growth of graphene layers: Transmission electron microscopy and density functional theory studies*, arxiv.org, Cornell University run website, 2011.

[4]. A.V. Sinelnik, A.V. Semenov, *Theoretical study of the band structure of 2H-SiC and 4H-SiC of silicon carbide polytypes*, Condensed Matter Physics, 2021. 24(2), p. 23706-1 to 6.

[5]. N.G.C. Astrath, A.C. Bento, M.L. Baesso, A. Ferreira de Silva, C. Persson, *Photoacoustic spectroscopy to determine the optical properties of thin film 4H-SiC*, Thin Solid Films, 2006. 515, p. 2821-2823.

Journal of Research in Engineering and Computer Sciences
August 2023, Vol. 1, No. 3, pp. 43-66

Analysis of the Influence of the Water/Graphene Nanofluid as Working Fluid on the Thermal Performance of Finned Heat Pipes Used in Air Conditioning

Élcio Nogueira

1. Department of Mechanic and Energy, State University of Rio de Janeiro, Brazil

Abstract:
This is a theoretical analysis of the influence of fractions of graphene nanoparticles associated with distilled water as a working fluid in a heat exchanger used in an air conditioning system for operating rooms. The heat exchanger consists of a set of finned heat pipes. Theoretical results are confronted with experimental results for water as the working fluid. The analysis is restricted to the evaporator since the nanoparticles do not influence the results in the condenser heat exchanger. The thermal efficiency method is applied to obtain the results. The analysis presents results for air velocity, Nusselt number for air, overall evaporator heat exchange coefficient, evaporator Nusselt number, evaporator thermal effectiveness, and the air outlet temperature. It was determined that the influence of fractions of graphene nanoparticles is not significant on the evaporator heat exchanger analyzed. Despite this, it is observed that smaller fractions of nanoparticles have a greater influence on thermal performance and there is an upper limit for volume fractions.

Keywords: Finned heat pipes, water/graphene nanofluid, air conditioning, boiling heat transfer correlations, thermal efficiency method.

INTRODUCTION

The objective is to apply the analytical thermal efficiency method to analyze the influence of graphene particles on the performance of the heat pipe system in the evaporator of the heat exchanger studied by Ragil Sukarno [1]. The Figures below show the heat pipe system in the evaporator and condenser, and how they are in a staggered configuration in rows of 4 pipes. The original working fluid is water and has a saturation temperature of 27°C.

The system used in the experiment carried out for the thermal analysis of the heat exchanger consists of sets of 12, 24, and 36 finned heat pipes, as shown in Figure (1.a), Figure (1.b) and Figure (1. c). The experiment was carried out by Ragil Sukarno et al. [1], who used the effectiveness method (ε-NTU) for global analysis of the heat exchanger. The finned heat pipe heat exchanger (FHPHE) has a staggered configuration consisting of three, six, and nine rows of heat pipes. The air inlet temperature in the evaporator ranges from 30.0°C to 45°C. The airflow ranges from 0.05 kg/s to 0.095 kg/s.

Nandy Putra et al. [2] experiment with heat recovery using finned heat pipes, with water as the working fluid, in an air conditioning system. They analyze the influence of the number of heat pipes, inlet temperature, and inlet air velocity. They determine that finned heat exchanger performance strongly depends on air velocity and that higher inlet velocity enables better performance.

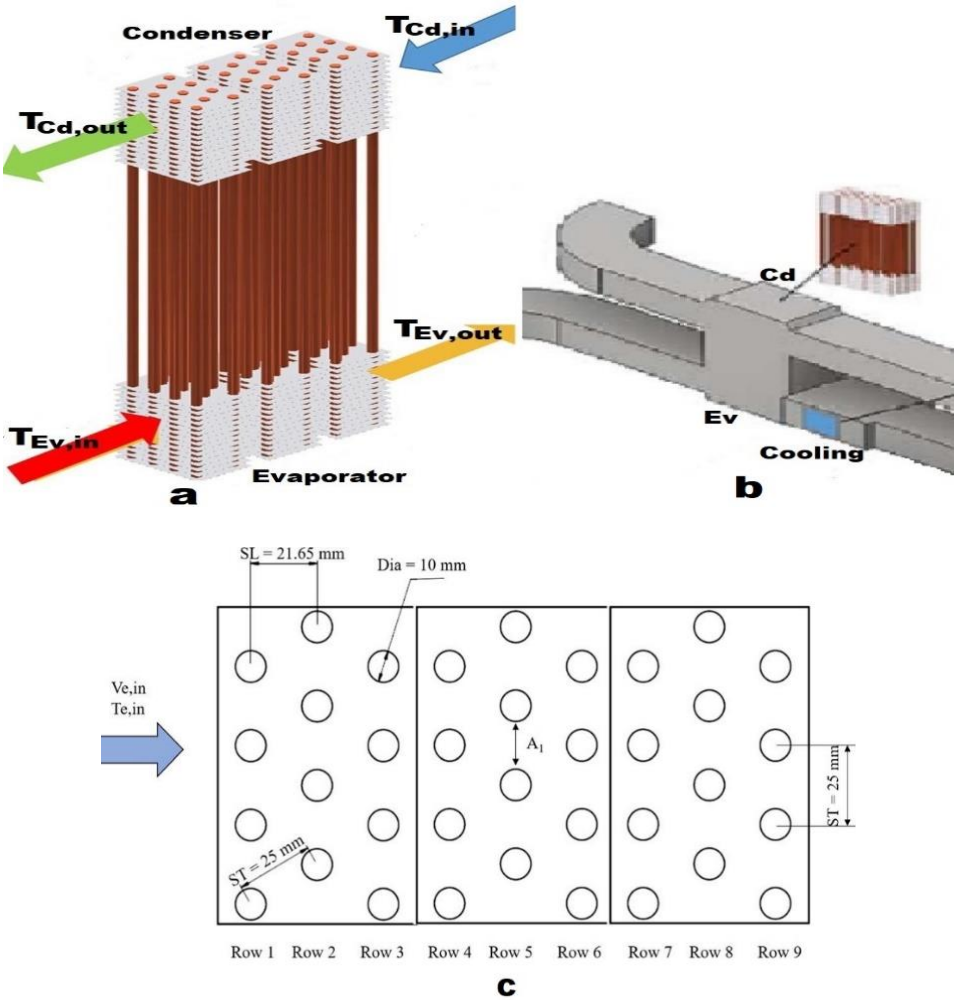

Figure (1. a) represents the set of finned heat pipes [1]; Figure (1. b) represents the evaporator (pre-cooling), conventional cooling, condenser (energy recovery), and air circulation pipes [1]; Figure (1. c) schematically represents the set of finned heat pipes arranged in the heat exchanger shell [1].

Grzegorz Górecki et al. [3] study a small air-conditioning system consisting of individually finned heat pipes using R404 refrigerant as the working fluid. Theoretical-experimental work makes it possible to conclude that individual fins are an alternative to conventional heat exchangers and that they are less susceptible to deformation and easy to replace and clean.

H. Jouhara et al. [4] uses a finned tube heat exchanger consisting of multiple passes. The theoretical-experimental study aims at heating water using heated air, that is, recovery of residual energy. They use two theoretical methods for determining thermal quantities and comparing them with experimental results. It is a global implementation of the heat exchanger, and the methods used by them were the Log Mean Temperature Difference Method (LMTD) and the Effectiveness Method (ε-NTU). They report the significant importance of the Reynolds number in thermal performance.

Khaled Elsaid et al. [5] present a discussion related to the use of graphene as a nanofluid component with a focus on thermophysical properties. They argue that nanofluids using graphene have higher thermal conductivity than most nanofluids using metallic oxides and present a table of properties for comparison. However, they point out that there are major

challenges related to its use. They cite cost, stability, higher values for density and viscosity, environmental impacts, and preparation methods. They conclude that such challenges require careful investigation.

Naser Ali [6] studies characteristics related to graphene, such as thermophysical properties, and dispersion stability. It presents values for density, thermal capacity, thermal conductivity, and viscosity, in graphic form, for a nanofluid composed of water and graphene, with percentage values of volume fraction equal to 0.01%, 0.05%, and 0.10%. He argues that a feasibility study of the presented nanofluid is necessary before being used in real applications. Emphasizes cost, performance evaluation, and environmental impact aspects. It also analyzes the use of surfactants related to the stability of the nanofluid and concludes that stability of 45 days can be reached when using higher-weight surfactants.

The performance of thermosiphons can be improved with the use of nanofluids, as argued by A. Kamyar et al. [7]. They present a study to corroborate their statements and use two nanofluids using water mixed with Al_2O_3 and $TiSiO_4$ nanoparticles, with volume fractions equal to 0.01%, 0.05% and 0.07%. The results presented demonstrate that there is a reduction in thermal resistance and an improvement in the performance of the thermosiphons. They emphasize that the boiling coefficient increases with the use of nanoparticles in thermosiphons and, as a numerical argument, they use the Merit number that makes it possible to determine the relative effect of the properties of the nanofluid. However, they consider that the performance of thermosiphons depends on particle size, particle type, bubble nucleation size, and base fluid.

Agnieszka Kujawska et al. [8] state that the performance of the condenser is not influenced by the nanofluids used in the heat pipe and that the performance analysis should be concentrated on the evaporator. They analyze the surface tension and contact angle of silica and graphene oxide nanofluids and argue that nanoparticles tend to deposit on the surface of the evaporator during the boiling process. This deposit alters the conditions in the wall and in the region close to it, and the effect this may have on the nanofluid properties is unknown. It is known, however, that changes in surface tension and wettability affect the boiling regime. The study presents numerical results for the surface tension of graphene oxide before and after the boiling process, with water as the base fluid. They also analyze the influence of surfactants on the surface tension associated with the nanofluid. They conclude that graphene has surface tension and contact angle similar to water, when in small concentrations and state, citing references, that the impact of graphene oxide on heat transfer capacity is not related to surface tension or wettability. However, they add, more research is needed to determine the influence of the use of nanofluids in thermosyphons at the boiling process, and that the studies carried out are rarely associated with real applications, especially in low-pressure devices.

Amir Akbari et al..[9] state that the use of nanofluids related to an increase in nucleated boiling has aroused great interest. They carried out an experimental study conducted under atmospheric pressure to compare the effects of graphene nanoplatelets and multi-walled carbon nanotubes on the heat transfer coefficient associated with pool boiling and the critical heat flux. They verified that nanoparticles with percentage concentrations in weight equal to 0.01, 0.05, and 0.1% altered the heat transfer coefficient and the critical heat flux, about deionized water. Concentrations above 0.01% by weight decreased the heat transfer coefficient and increased the critical heat flux. Furthermore, they experimentally demonstrated that the thermal conductivity of nanofluids and

the functionalization method (non-covalent and covalent) directly affect the heat transfer coefficients and the critical heat flux.

Jaqueline Barber et al. [10] published a review related to recent advances in pool boiling and convective boiling related to the use of nanofluids. The review work focused on the improvement and degradation in the nucleate boiling heat transfer coefficient and critical heat flux and concluded that there are conflicting data published in the literature presented in tabular form. They found that most of the work reports that the deposition of nanoparticles on the surface of the heat exchanger is related to an increase in the critical heat flux with the use of nanofluids.

K. N. Shukla et al. [11] present experimental work with a cylindrical copper heat pipe filled with different working fluids. They performed tests with deionized water, and nanofluids composed of silver-aqua and copper-water. They found a 14% increase in heat pipe efficiency with the use of nanofluids compared to deionized water as the working fluid. They observed an increase in the thermal conductivity of nanofluids with 0.1% by weight of nanoparticles. They find that nanoparticles can create several active nucleation sites, enabling an increase in heat transfer by boiling, with a consequent decline in the temperature profile.

Kapilan Natesan and Shashikantha Karinka[12] argue that the use of energy in its various forms is vital for the development of any country. They add that it is one of the most used devices in heat transfer applications and that any effective improvement of heat exchange between fluids brings benefits. They claim that the solid particles have higher thermal conductivity than the usual working fluids used in heat pipes and can improve the efficiency of heat exchangers. They mention that graphene-based nanoparticles have high thermal conductivity, low erosion, and enable an increase in the heat transfer rate. This improvement in heat transfer can lead to equipment downsizing in different types of applications. In this sense, the review highlights the advantages of using graphene, for example, in electronic devices.

Mohammed Salah Hameed [13] recognizes that there are four correlations frequently used to simulate nucleate boiling and that each of them is differentiated by the variables used in its implementation. With the objective of improving the precision in the determination of the boiling heat transfer coefficient, they develop a generalized empirical correlation that satisfies a wide range of experimental data available in the literature. They use the least squares multiple regression techniques to determine a correlation that allows minimum deviation. They test the correlation developed by the linear and non-linear programming solution and using a wide range of literature data presented by Rohsenow, Forster and Zuber, Forster and Greif, and Gupta and Varshney.

Suriyawong et al. [14] present a study where they developed a new correlation for predicting the nucleate pool boiling heat transfer coefficient of TiO_2-Water nanofluids for low concentrations. The proposed correlation considers several relevant factors. They use data obtained from studies that show correlations associated with nanofluid properties and develop a correlation that predicts results with good accuracy for the copper surface but with poor accuracy for the aluminum surface.

Élcio Nogueira [15] applied the second law of thermodynamics through the concepts of thermal efficiency, thermal effectiveness, and thermal irreversibility in a shell and tube heat exchanger utilizing a water-ethylene glycol associated with fractions of nanoparticles. Volume fractions

equal to 0.01, 0.10, and 0.25 were considered for analysis for nanoparticles of Ag and Al_2O_3. He concluded that, when the Reynolds number is relatively small in a laminar regime, high effectiveness, associated with high thermal irreversibility, leads to heat transfer rates that approach the maximum possible.

Élcio Nogueira [16] states that the thermal efficiency method, associated with viscous irreversibility and the thermodynamic Bejan number, enables analysis of the optimization of heat exchangers. It applies the method to the cooling of machine oil in a heat exchanger with external fins associated with the tubes. He includes spherical nanoparticles of Boehmite Alumina in the analysis, concluding that the inclusion of nanofluid presents a significant improvement in thermal performance, associated with an increase in viscous dissipation, and a decline in the Bejan number.

Élcio Nogueira [17] analyzes the influence of the thermal performance of a shell and tube-type condenser, with water and aluminum oxide (Al_2O_3) nanoparticles flowing into the tube. The principles parameters used to analyze the thermal performance are thermal efficiency and thermal effectiveness, and the results demonstrate that efficiency is high and that the effectiveness can be increased by introducing fractions of nanoparticles in the water.

METHODOLOGY

The formulation below, Equations (1) – (91) is related to the thermal performance of the heat exchanger analyzed by Ragil Sukarno et al. [1], represented through Figures 1.a, 1.b and 1.c. Graphene volume fractions are represented by the parameter ϕ which ranges from 0.001 to 0.100.

$$T_{sat} = 27.0\,^{o}C \;\; fixed \tag{1}$$

$$T_{airin} = 30\,^{o}C \;\; default,\; 30^{o}C \le T_{airin} \le 45^{o}C \tag{2}$$

$$T_W = T_{airin} \;\; by\ definition \tag{3}$$

T_{sat} is the saturation temperature of the working fluid, T_{airin} is the air inlet temperature, T_W is the surface temperature of the heat pipe.

$$\phi = 0.01 \;\; default,\; 0.001 \le \phi \le 0.100$$

ϕ is the volume fraction of the nanofluid

$$k_{air} = 6.9174418\,10^{-5} Tair_{in} + 0.02462173663 \tag{4}$$

$$\mu_{air} = 1.9548362\,10^{-5} + 2.73505803\,9\,10^{-9} Tair_{in} + 2.30958747\,9\,10^{-10} Tair_{in}^2 - 4.50588235\,3\,10^{-13} Tair_{in}^3 \tag{5}$$

$$Cp_{air} = 1003.728948 + 0.06727399886 * Tair_{in} + 3.565918367\,10^{-6} Tair_{in}^2 + 8.222222222\,10^{-7} Tair_{in}^3 \tag{6}$$

$$\rho_{air} = 1.219135515 - 0.002152770329 Tair_{in} - 3.6404747910^{-7} Tair_{in}^2 + 1.7058823510^{-9} Tair_{in}^3 \quad (7)$$

$$\nu_{air} = \frac{\mu_{air}}{\rho_{air}} \quad (8)$$

$$\alpha_{air} = \frac{k_{air}}{\rho_{air} Cp_{air}} \quad (9)$$

$$\mathrm{Pr}_{air} = \frac{\nu_{air}}{\alpha_{air}} \quad (10)$$

Equations (4-10) represent the properties of air at the air inlet temperature.

$$k_W = 0.5521904762 + 0.002561507937 T_W - 1.872023810^{-5} T_W^2 + 5.9027777810^{-8} T_W^3 \quad (11)$$

$$Cp_W = 4217.8 - 3.412833333 T_W + 0.109375 T_W^2 - 0.0016890625 T_W^3 + 1.3437510^{-5} T_W^4 - 4.08854166710^{-8} T_W^5 \quad (12)$$

$$\rho_W = 1002.676071 - 0.06559821429 T_W - 0.003582589286 T_W^2 \quad (13)$$

$$\nu_W = 1.78766666710^{-6} - 5.53222222210^{-8} T_W + 9.8270833310^{-10} T_W^2 - 8.9652777810^{-12} T_W^3 + 3.1770833310^{-14} T_W^4 \quad (14)$$

$$\mu_W = \rho_W \nu_W \quad (15)$$

$$\alpha_W = \frac{k_W}{\rho_W Cp_W} \quad (16)$$

$$\mathrm{Pr}_W = \frac{\nu_W}{\alpha_W} \quad (17)$$

Equations (11-16) represent the properties of water at the heat pipe.

$$P_{sat} = 216.7691429 - 5.927342857 T_{sat} + 0.04774285714 T_{sat}^2 \quad (18)$$

P_{sat} is the saturation pressure of the working fluid.

$$\nu_l = 0.001585485714 - 1.831904762\,10^{-5} T_{sat} + 1.957142857\,10^{-7} T_{sat}^2 - 6.666666667\,10^{-10} T_{sat}^3 \quad (19)$$

$$\rho_l = \frac{1}{\nu_l} \quad (20)$$

$$\nu_V = 21.45466571 - 0.3398517143 T_{SAT} + 0.001419714286 T_{sat}^2 \quad (21)$$

$$\rho_v = \frac{1}{\nu_v} \quad (22)$$

Equations (19-22) represent the properties of the saturated liquid and saturated vapor in the heat pipe.

$$h_l = 2.184 + 4.2124 T_{sat} \quad (23)$$

$$h_v = 1.540666667 T_{sat} + 2521.596667 \quad (24)$$

$$h_{lv} = h_v - h_l \quad (25)$$

h_{lv} represents the latent heat of vaporization.

$$NHP = 12\ default; 12 \le NHP \le 36 \quad (27)$$

NHP is the number of heat pipes associated with the heat exchanger.

$$NFin = 30\ default;\ 0 \le NFin \le 30 \quad (28)$$

$NFin$ is the number of fins per heat pipe.

$$NHP_{byrows} = 4 \quad (29)$$

NHP_{byrows} is the number of heat pipes per row.

$$Nrows = \frac{NHP}{NHP_{byrows}},\ 3 \le Nrows \le 9 \quad (30)$$

$Nrows$ is the number of rows in the heat exchanger.

$$Vair_{inlet} = 1.5\ m/s\ default\ ;\ 1.5 \le Vair_{inlet} \le 2.5 \tag{31}$$

$Vair_{inlet}$ is the air velocity at the evaporator inlet.

$$\dot{m}_{air} = 0.050\ kg/s\ default;\ 0.050 \le \dot{m}_{air} \le 0.095 \tag{32}$$

$\dot{m}_{air}$ is the mass flow rate of air.

$$TEv_{in} = T_{airin};\ 30.0^{o}C \le TE_{in} \le 45.0^{o}C \tag{33}$$

$$\sigma_{Water} = 0.07275\left(1 - 0.002\left(368.15 - 291.15\right)\right) \rightarrow \textit{valid for water} \tag{34}$$

σ_{Water} is the surface tension associated with water.

$$r = 0.33 \tag{35}$$

$$C_{sf} = 0.015 \tag{36}$$

$$C_{sf}^{*} = 1503 \tag{37}$$

$$l^{*} = \sqrt{\left(\frac{\sigma_{Water}}{g(\rho_l - \rho_v)}\right)} \tag{38}$$

l^{*} is the characteristic length.

$$q'' = \mu_W h_{lv} l^{*} \left(\frac{1}{Csf}\right)^{0.33} Pr_W^{\,1/r} \left(\frac{\sigma_{Water} \Lambda T_{sat}}{h_{lv}}\right)^{1/r} \tag{39}$$

q'' is the heat flux associated with the boiling process based on the equation obtained by Rhosenow[18].

$$h_{boil} = 1.39\left(\frac{k_W}{l^{*}}\right)\left(\frac{q'' \rho_W Cp_W l^{*}}{\rho_W h_{lv} k_W}\right)^{0.7}\left(\frac{\rho_l}{\rho_v}\right)^{0.21}\left(\frac{\mu_W Cp_W}{k_W}\right)^{-0.21} \rightarrow \text{valid for water} \tag{40}$$

h_{boil} Equation (40), an expression developed by Gupta and Varshney, is the heat transfer coefficient associated with the boiling process valid for water [13].

$$\rho_{Grap} = 3000\ kg/m^{3} \tag{41}$$

$$k_{Grap} = 2500\ W/(mK) \tag{42}$$

$$Cp_{Grap} = 711\ J/(kgK) \tag{43}$$

$$\mu_{nano} = (1-\phi)^{-2.5}\mu_W \tag{44}$$

$$\rho_{nano} = \phi\rho_{Grap} + (1-\phi)\rho_W \tag{45}$$

$$Cp_{nano} = \frac{\phi\rho_{Grap}Cp_{Grap} + (1-\phi)\rho_W Cp_W}{\rho_{nano}} \tag{46}$$

$$k_{nano} = [\frac{k_{Grap} + 2k_W + 2(k_{Grap} - k_W)(1+0.1\phi)^3\phi}{k_{Grap} + 2k_W - 2(k_{Grap} - k_W)(1+0.1\phi)^2\phi}]k_W \tag{47}$$

$$\mu_{nano} = \rho_{nano}\nu_{nano} \tag{48}$$

$$\alpha_{nano} = \frac{k_{nano}}{\rho_{nano}Cp_{nano}} \tag{49}$$

$$\mathrm{Pr}_{nano} = \frac{\nu_{nano}}{\alpha_{nano}} \tag{50}$$

$$\sigma_{nano} = 0.0726505555 - 1.621336444d - 5*Tsat - 1.367231268d - 6*Tsat**2.0 \tag{51}$$

σ_{nano} is the surface tension associated with nanofluid [7].

$$\varepsilon = 0.210^{-6} \tag{52}$$

ε is the surface roughness [15].

$$h_{boil} = 28.85\,Pr_{nano}^{0.59}(\frac{q''\varepsilon}{\mu_{nano}h_{lv}})^{0.70}(\varepsilon^2 g(\frac{\rho_{nano} - \rho_v}{\sigma_{nano}}))^{0.16}(\frac{k_{nano}}{\varepsilon(\phi + 0.001)}) \rightarrow \text{valid for nanofluid} \tag{53}$$

h_{boil} Equation (53) is the heat transfer coefficient associated with the boiling process valid for nanofluid [14].

$$\Delta T_{Evsat} = TEv_{in} - T_{sat} \tag{54}$$

$$D_{ext} = 10.3 10^{-3}\ m \tag{55}$$

$$D_{\text{int}} = 10.0 10^{-3}\ m \tag{56}$$

D_{ext} is the outer diameter of the heat pipe. D_{int} is the inner diameter of the heat pipe.

$$kW = 401.0\, W/(mK) \tag{57}$$

kW is the thermal conductivity of the heat pipe material (copper).

$$LEv = 160.010^{-3} \tag{58}$$

LEv is the length of the evaporator.

$$LEv_H = N_{Rows}\frac{LEv}{9.0} \tag{59}$$

LEv_H is the horizontal length of the heat exchanger.

$$t_{Fin} = 0.10510^{-3} \tag{60}$$

t_{Fin} is the thickness of the fins.

$$k_{Fin} = 235.0 \tag{61}$$

k_{Fin} is the thermal conductivity of the fin material.

$$Sp_{Fin} = 2.0 10^{-3}\ by\ definition \tag{62}$$

Sp_{Fin} is the distance between fins.

$$LEv_{effec} = LEv - (NFin\, t_{Fin} + 4\pi D_{ext} Sp_{Fin}) \tag{63}$$

LEv_{effec} is the effective length of the evaporator.

$$Dh_{EV} = \frac{4\, LEv_H\, LEv_{effec}}{2(LEv_H + LEv_{effec})} \tag{64}$$

Dh_{EV} is the hydraulic diameter of the evaporator.

$$\mathrm{Re}_{Ev} = \frac{4\dot{m}_{air}}{\pi Dh_{Ev}\mu_{air}} \tag{65}$$

Re_{Ev} is the Reynolds number associated with the evaporator.

$$A\mathrm{sec}_{Ev} = \frac{\dot{m}_{air} Dh_{Ev}}{\mathrm{Re}_{air}\ \mu_{air}} \tag{66}$$

$A\mathrm{sec}_{Ev}$ is the cross-sectional area associated with the evaporator.

$$V_{Ev} = \frac{\dot{m}_{air}}{A\mathrm{sec}_{Ev}\ \rho_{air}} \tag{67}$$

V_{Ev} is the air velocity in the evaporator.

$$ST = 25.010^{-3} \tag{68}$$

$$SL = 21.6510^{-3} \tag{69}$$

ST and SL are lengths associated with the set of heat pipes (Figure 1.c).

$$Vair_{\max} = \frac{ST}{SL - Dext} Vair_{inlet} \tag{70}$$

$Vair_{\max}$ is the maximum air velocity in the evaporator.

$$Atr_{EvFin} = NFin\, LEv_H\ LEv \tag{71}$$

Atr_{EvFin} is the heat rock area associated with fins.

$$Atr_{EvHP} = NHP\, \pi D_{ext} (LEv - NFin\, Sp_{Fin}) \tag{72}$$

Atr_{EvHP} is the heat exchange area associated with the heat pipes.

$$A_{EvTotal} = Atr_{EvFin} + Atr_{EvHP} \tag{73}$$

$A_{EvTotal}$ é a área de troca de calor total no evaporador.

$$Nu_{Ev} = F\, 0.71 \mathrm{Re}_{Ev}^{0.5}\, \mathrm{Pr}_{Ev}^{0.36} \left(\frac{\mathrm{Pr}_{Evair}}{\mathrm{Pr}_{EvSurf}}\right)^{0.25} \tag{74}$$

Nu_{Ev} is the Nusselt number associated with the evaporator, where F=0.98 by definition.

$$h_{Ev} = \frac{Nu_{Ev} k_{air}}{Dh_{EV}} \tag{75}$$

h_{Ev} is the convection heat exchange coefficient.

$$mL_{EvFin} = \sqrt{\frac{2h_{Ev}}{k_{Fin} t_{Fin}}}\, LEv_{H} \tag{76}$$

mL_{EvFin} dimensionless parameter associated with the fins.

$$\eta_{EvFin} = \frac{\mathrm{Tanh}(mL_{EvFin})}{mL_{EvFin}} \tag{77}$$

η_{EvFin} is the efficiency associated with fins.

$$\beta_{Ev} = \frac{Atr_{EvFin}}{A_{Total}} \tag{78}$$

β_{Ev} is the ratio between the heat exchange area of the fins in relation to the total area.

$$\eta_{EvFin}^{'} = \beta_{Ev}\, \eta_{EvFin} + (1 - \beta_{Ev}) \tag{79}$$

$\eta_{EvFin}^{'}$ is the effective efficiency associated with the set of fins.

$$Uo_{Ev} = \frac{1}{\frac{1}{h_{boil}} + \frac{D_{ext} - D_{int}}{kW} + \frac{1}{\eta_{EvFin}^{'} h_{Evair}}} \tag{80}$$

Uo_{Ev} is the overall heat transfer coefficient associated with the evaporator.

$$C_{Air} = \dot{m}_{air} Cp_{air} \tag{81}$$

$$C_{Ev} = C_{air} \tag{82}$$

C_{Air} is the heat capacity of air.

$$NTU_{Ev} = \frac{Uo_{Ev} A_{EvTotal}}{CEv} \tag{83}$$

NTU_{Ev} is the number of thermal units associated with the evaporator.

$$Fa = \frac{NTU\sqrt{1+C^{*2}}}{2} \; for\; cross-flow \tag{84}$$

Fa is a dimensionless parameter called "Analogy of Fins", associated with the efficiency method [16-18]. $C^* = \frac{C_{min}}{C_{max}} = 0$ to the evaporator ($C_{max} \to \infty$).

$$\eta_T = \frac{tanh(Fa)}{Fa} \tag{85}$$

η_T is the thermal efficiency associated with the heat exchanger.

$$\varepsilon_T = \frac{1}{\frac{1}{\eta NTU} + \frac{1+C^*}{2}} \tag{86}$$

ε_T is the thermal effectiveness associated with the heat exchanger.

$$Fa_{Ev} = \frac{NTU_{Ev}}{2} \tag{87}$$

$$\eta_{TEv} = \frac{tanh(Fa_{Ev})}{Fa_{Ev}} \tag{88}$$

$$\varepsilon_{TEv} = \frac{1}{\frac{1}{\eta_{TEv} NTU_{Ev}} + \frac{1}{2}} \tag{89}$$

$$\dot{Q}_{Ev} = \frac{C_{Ev} \Delta T_{Evsat}}{\frac{1}{\eta_{TEv} NTU_{Ev}} + \frac{1}{2}} \tag{90}$$

$\dot{Q}_{Ev}$ is the rate of heat transfer in the evaporator.

$$TEv_{out} = TEv_{in} - \frac{\dot{Q}_{Ev}}{C_{Ev}} \tag{91}$$

TEv_{out} is the outlet temperature of the air in the evaporator.

RESULTS AND DISCUSSION

The results presented below are related to the following parameters for analysis of the formulated problem: the number of heat pipes, the number of fins per heat pipe, air flow rate, air inlet temperature, and graphene volume fraction. The quantities of interest obtained in the analysis were the air velocity in the evaporator, the global heat transfer coefficient, the number of thermal units associated with the evaporator, the effectiveness of the evaporator, and the outlet temperature in the evaporator.

Figure 2 presents theoretical and experimental results[1] for air velocity in the evaporator, as a function of mass airflow rate. The parameters that vary are the number of heat pipes and the number of fins per heat pipe. The air velocity decreases with the increase of heat pipes and increases with the number of fins per heat pipe, that is, the area of the fins has a significant influence on the air velocity. The theoretical results are below the maximum experimental velocity value and the experimental evaporator velocity results are between the valid results for 12 and 24 heat pipes. There is, therefore, theoretical-experimental consistency in the results obtained.

Figure 3 shows values for the overall heat transfer coefficient, with air mass flow rate and graphene nanoparticle volume fraction as parameters. An increase in the coefficient is observed with the increase in the number of fins, and with the imposition of nanoparticles in the working fluid, with a volume fraction equal to 0.01%.

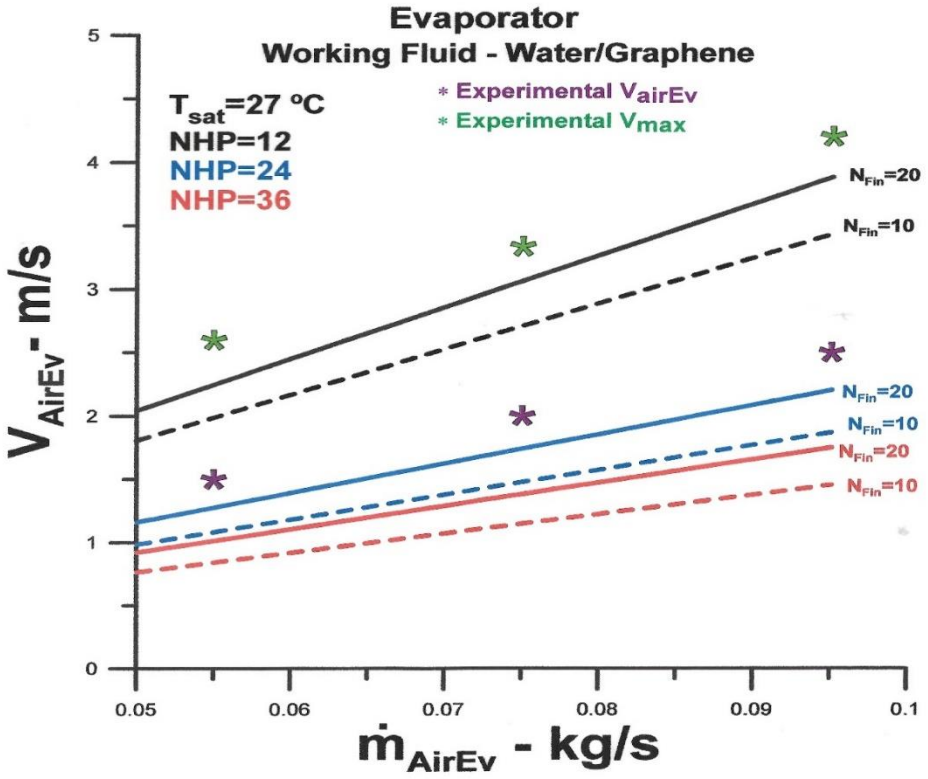

Figure 2: Evaporator air velocity versus mass air flow rate

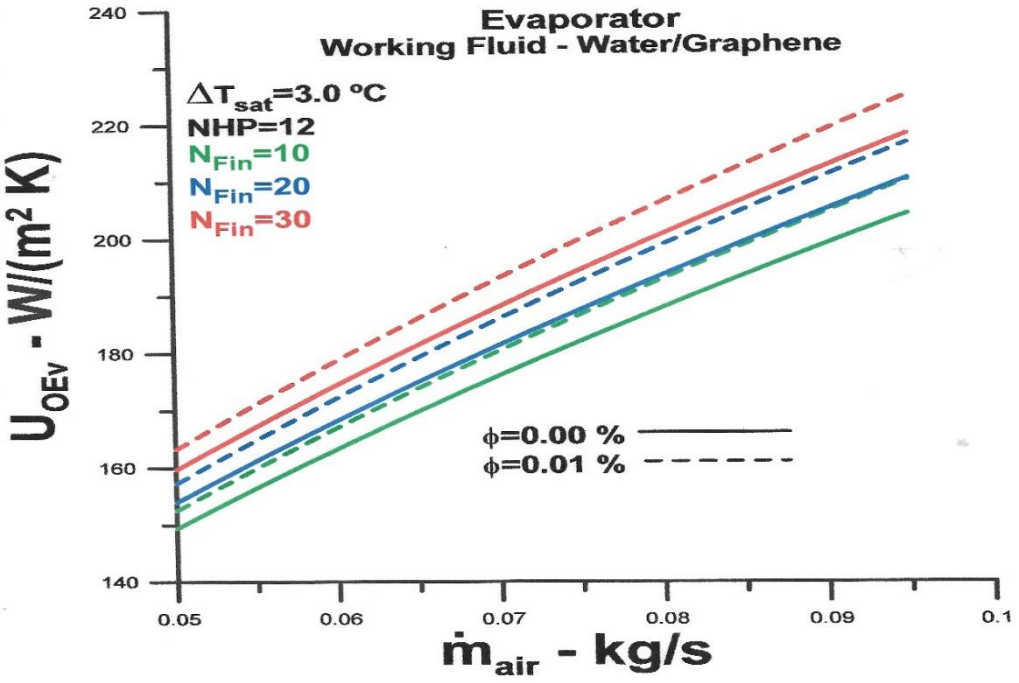

Figure 3: Evaporator Overall heat transfer coefficient versus mass air flow rate

Figure 4 shows that the number of thermal units in the evaporator grows with the number of fins and with the volume fraction of the nanofluid. The influence of nanoparticles, with a volume fraction equal to 0.01%, is more significant when there is an increase in the number of fins per heat pipe, that is when there is an increase in the heat exchange area. However, even for a larger number of fins, the relative difference between results with and without nanoparticles is small.

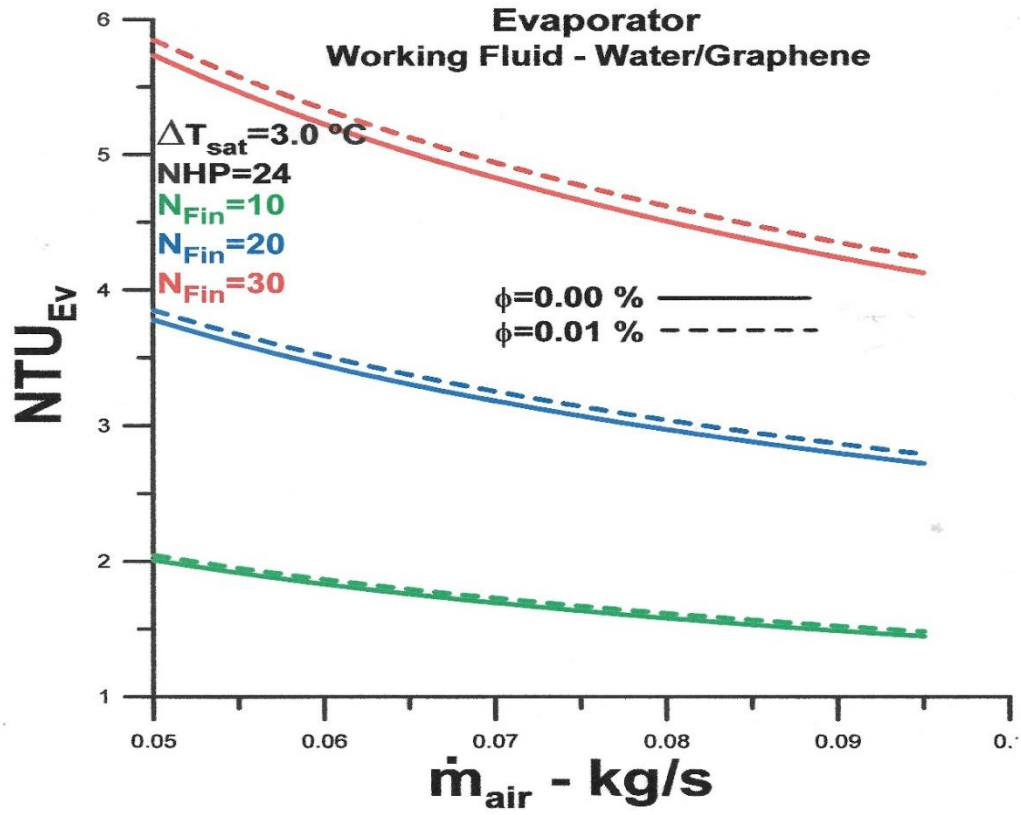

Figure 4: Evaporator number of thermal units versus mass air flow rate

Figure 5 presents results for effectiveness as a function of air mass flow rate and nanoparticles volume fraction, ϕ=0.01. Effectiveness decreases with increasing mass airflow rate. The effectiveness reaches a value very close to the maximum for NHP=24 and N_{Fin}=30, and there is no difference between with and without nanofluid. However, a slight difference can be observed when NFin=10. In practical terms, there is no advantage in using heat pipe values above 24, with 30 fins.

Figure 6 shows theoretical and experimental results for thermal effectiveness, with variation in air inlet temperature and ϕ =0.01. Effectiveness grows with the number of heat pipes and with the number of fins. When comparing situations with and without graphene nanoparticles, a slight increase in effectiveness is observed for lower inlet temperature values. However, the difference becomes almost imperceptible for a larger number of fins. Experimental results [1] are consistent with values obtained through the theoretical procedure.

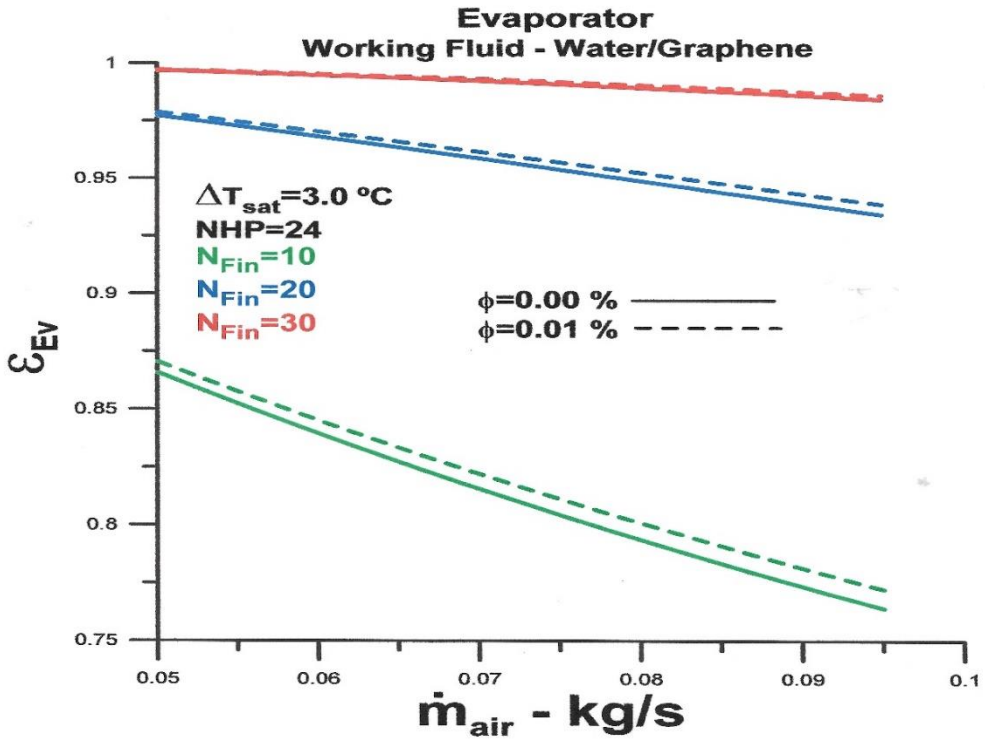

Figure 5: Thermal effectiveness number versus mass air flow rate

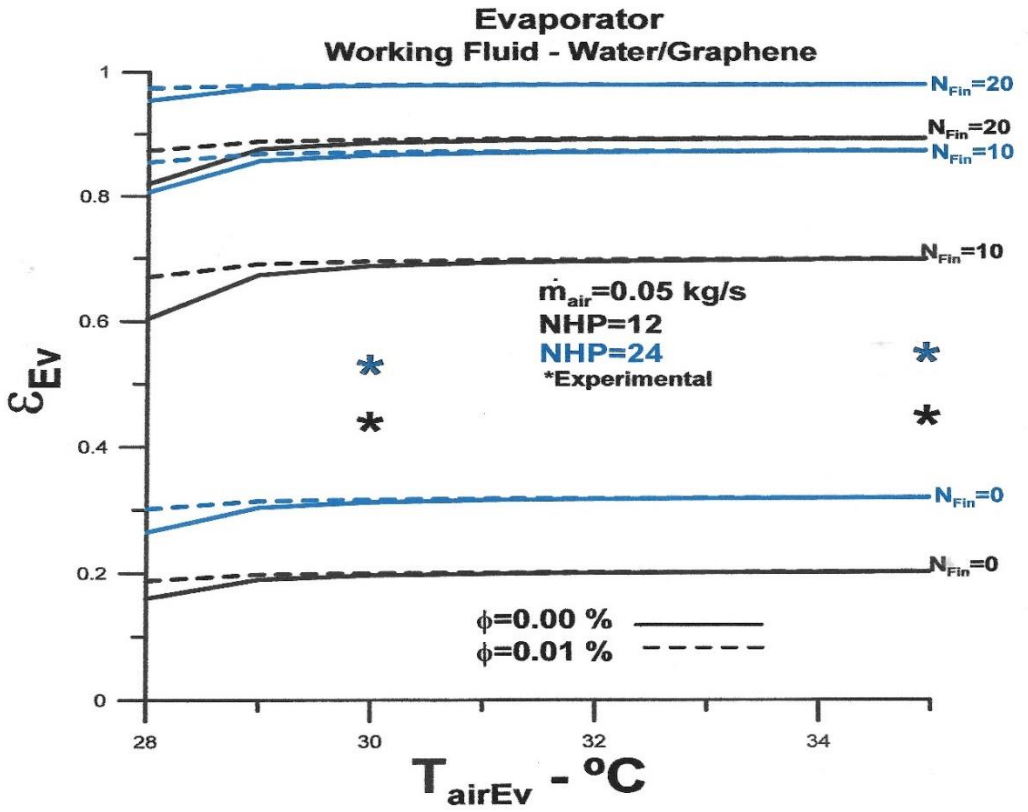

Figure 6: Evaporator thermal effectiveness versus inlet air temperature

The effectiveness versus volume fraction of the nanofluid is shown in Figure 7. Again, the effectiveness grows with the number of heat pipes and with the number of fins. However, there is no graphically perceptible variation in the effectiveness value in the analyzed volume fraction range. This result indicates that there is a saturation in the volume fraction value, that is, for the smallest volume fraction, equal to ϕ =0.01, the effectiveness has reached its highest possible value and there is no advantage in increasing the volume fraction. The questions raised by these results are: 1. Is there an advantage in decreasing the volume fraction value? 2. If so, what is the physical factor that causes the observed saturation, even for a low number of fins?

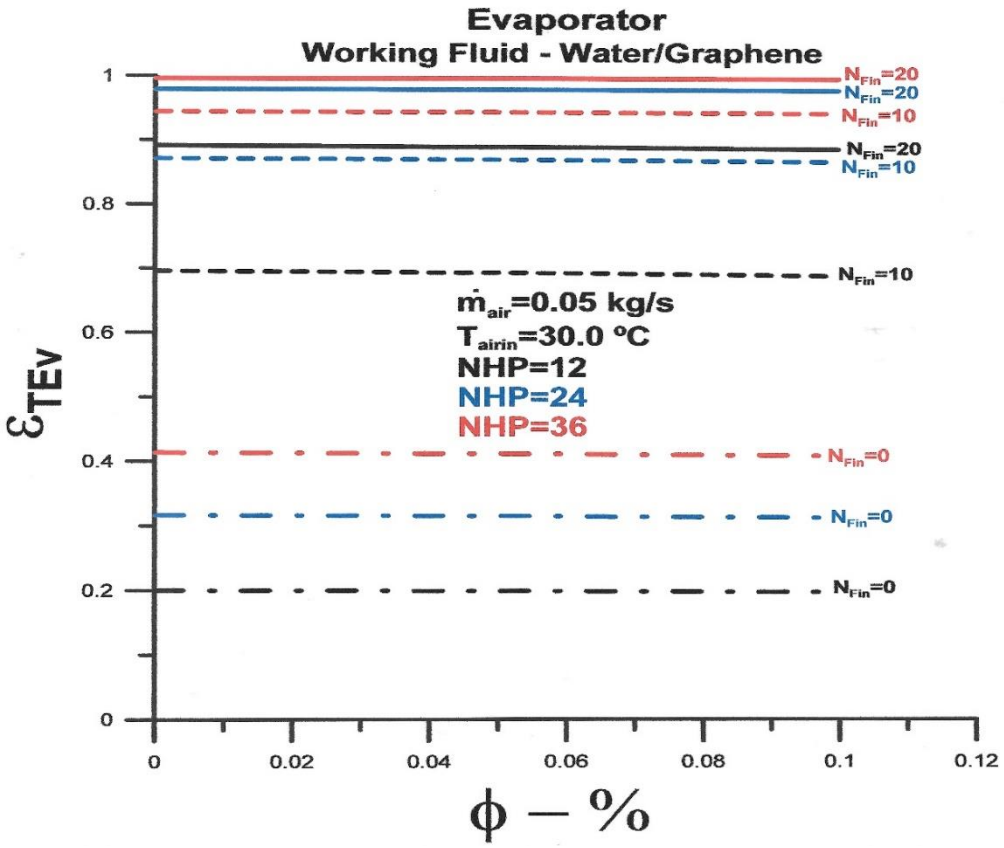

Figure 7: Evaporator thermal effectiveness versus nanofluid volume fractions

In order to try to answer the first question, values for effectiveness with lower values of fraction in volume are presented, in Figure 8. The results obtained are conclusive and demonstrate that lower values of fraction in the volume of the nanofluid allow higher values for effectiveness and that the value ϕ =0.01 is very close to the saturation point. Another interesting factor in the results presented in Figure 8 is that there is also a minimum limit for the volume fraction and that ϕ =0.005 is close to the lower limit for the analyzed configuration. Regarding the second question above, we can speculate, as there is evidence in the literature, that a possible cause for lower heat exchange performance lies in the deposition of nanoparticles on the heat pipe surface, thus increasing the thermal resistance.

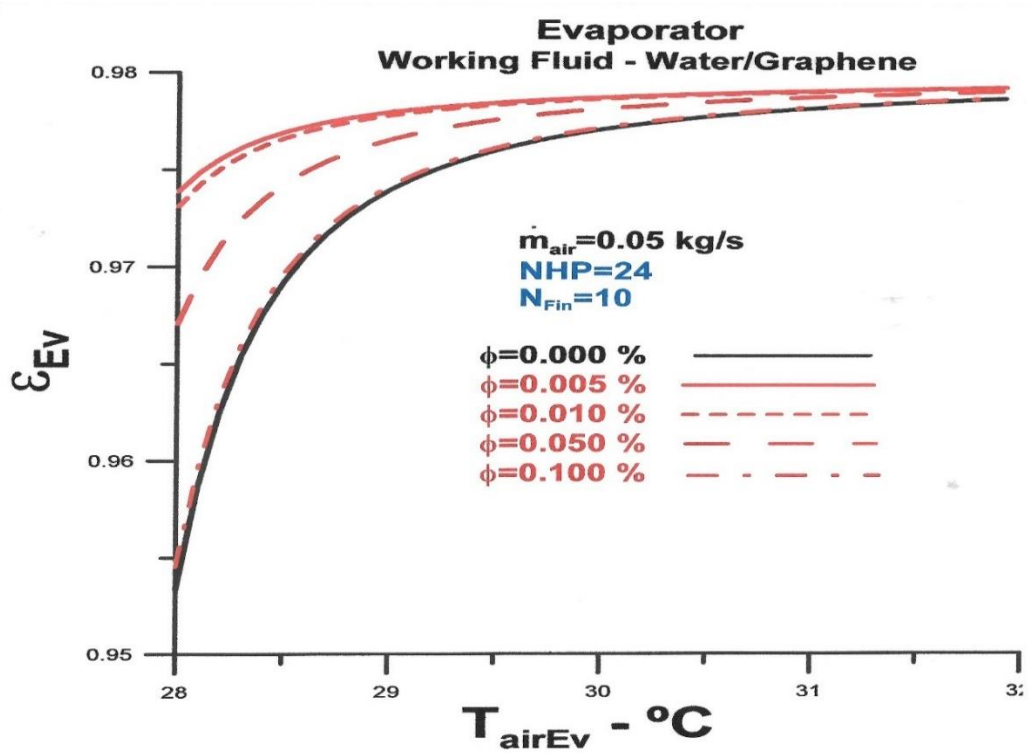

Figure 8: Evaporator thermal effectiveness versus inlet air temperature with nanofluid volume fractions as parameter

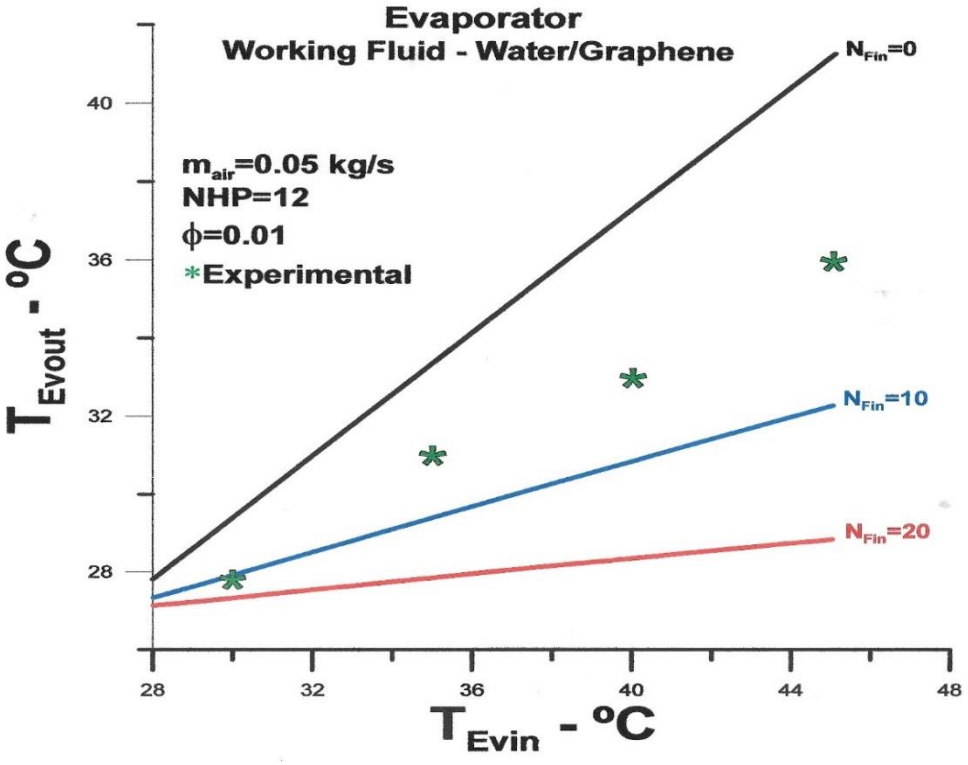

Figure 9: Outlet air temperature versus inlet air temperature

As expected, the results shown in Figure 9 corroborate the results obtained in Figure 5. The theoretical results in Figure 9 are associated with the volume fraction ϕ =0.01. Lower values for the outlet temperature of the air in the evaporator can be observed with the increase in the

number of heat pipes and fins. The experimental results [1] demonstrate consistency with the theoretical procedure.

Results from Figure 10 corroborate the results from Figure 7, as greater effectiveness lowers outlet temperature.

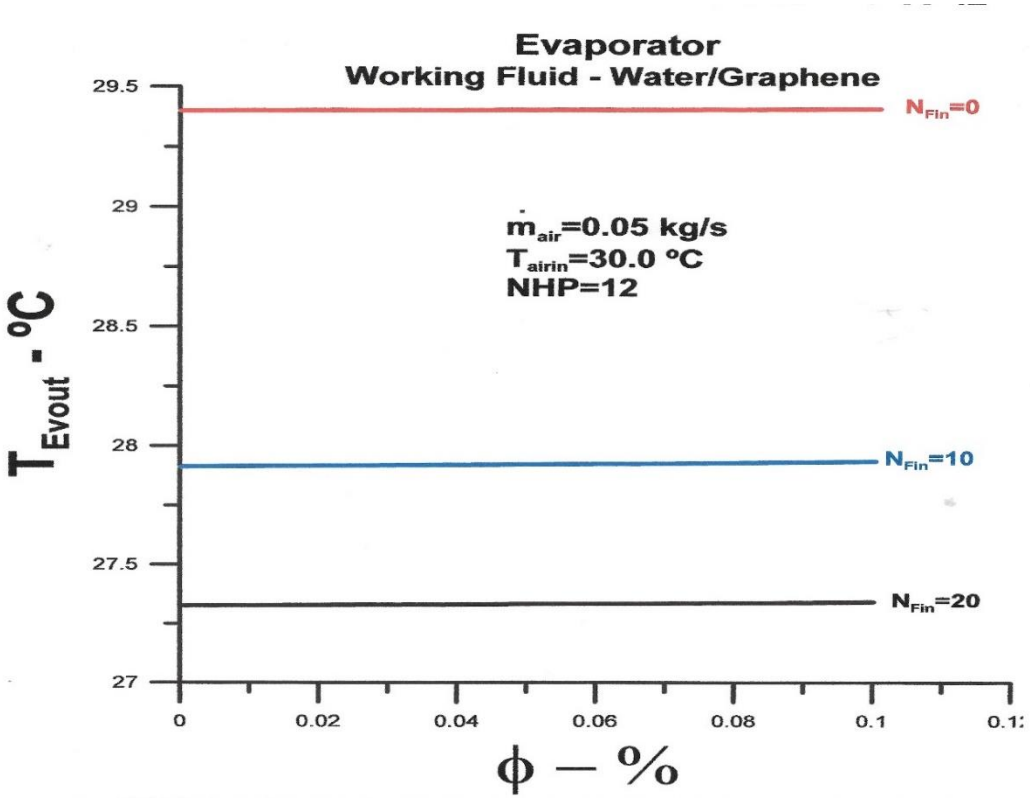

Figure 10: Outlet air temperature versus nanofluid volume fractions

Figures 11, 12, and 13 present results for outlet temperature for numbers of heat pipes respectively equal to 12, 24 and 36. The mass flow rates analyzed are 0.050 kg/s and 0.075 kg/s, with variations in volume fraction of 0.001 to 0.080. The results reinforce what has already been observed, that is, a smaller volume fraction allows a lower air outlet temperature. Although the values obtained for the three analyzed situations did not vary significantly, they demonstrate the importance of the number of heat pipes, associated with the number of fins. Furthermore, the data in Figure 13 demonstrate how the influence of the nanoparticle fraction in the working fluid occurs.

As already mentioned in the introduction, the evaluation of the role of nanofluids associated with heat pipes requires further studies that contribute to the various factors that affect thermal performance, especially for applications where the pressure field and the heat exchanged between the fluids are relatively low.

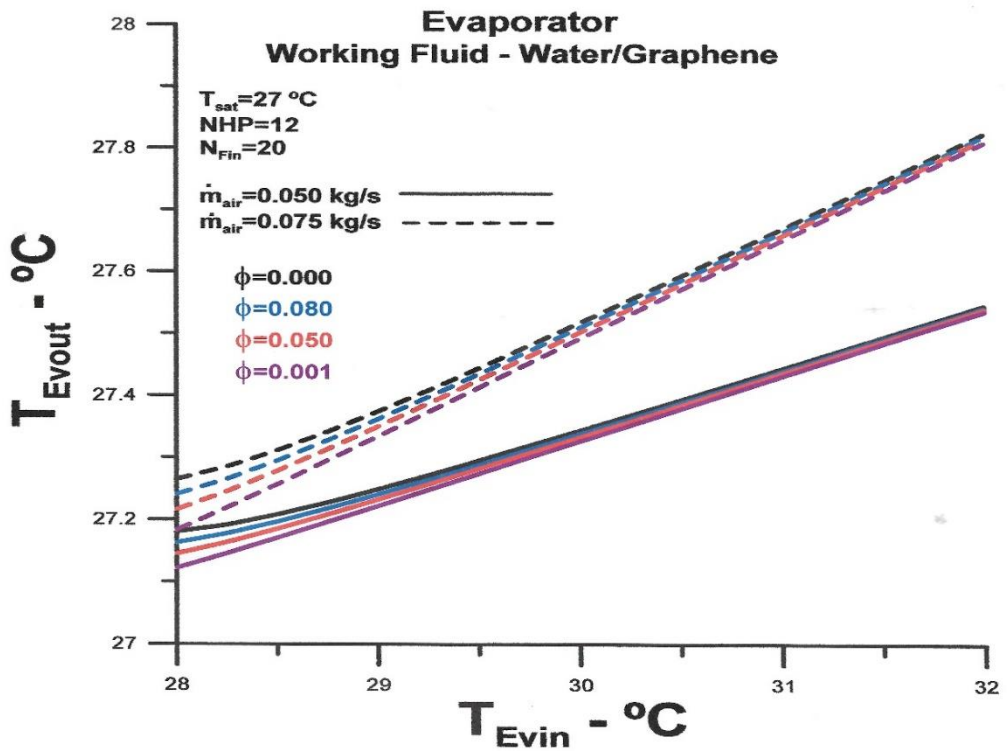

Figure 11: Outlet air temperature versus inlet air temperature for NHP=12 and N_{Fin}=20

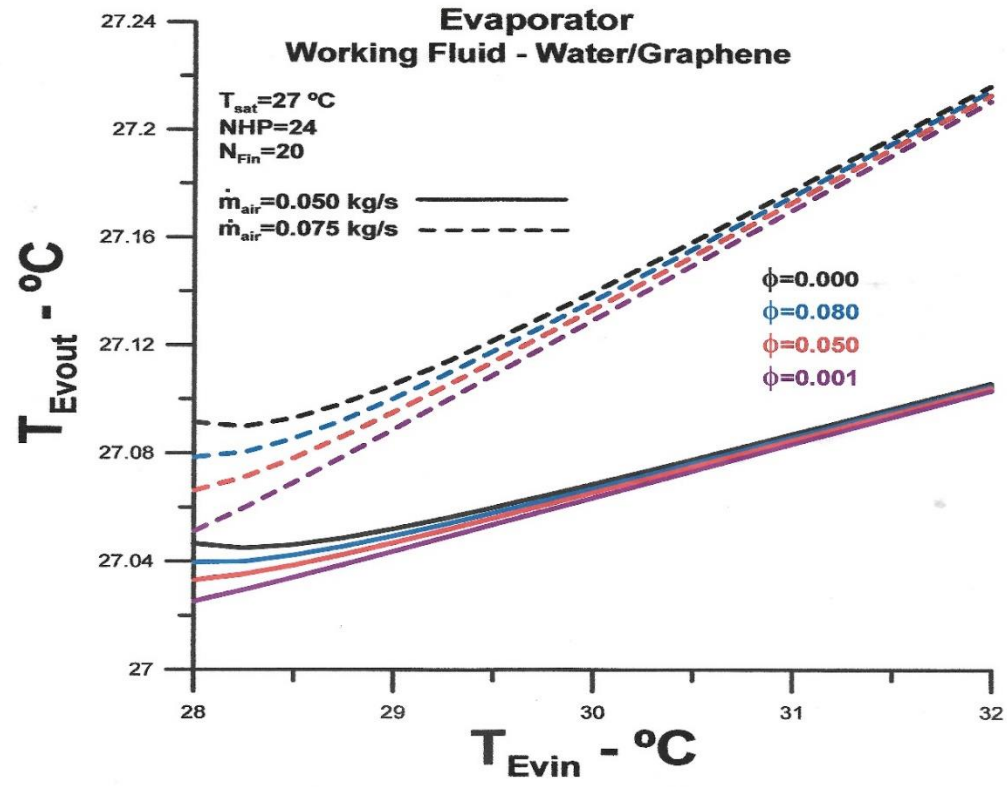

Figure 12: Outlet air temperature versus inlet air temperature for NHP=24 and N_{Fin}=20

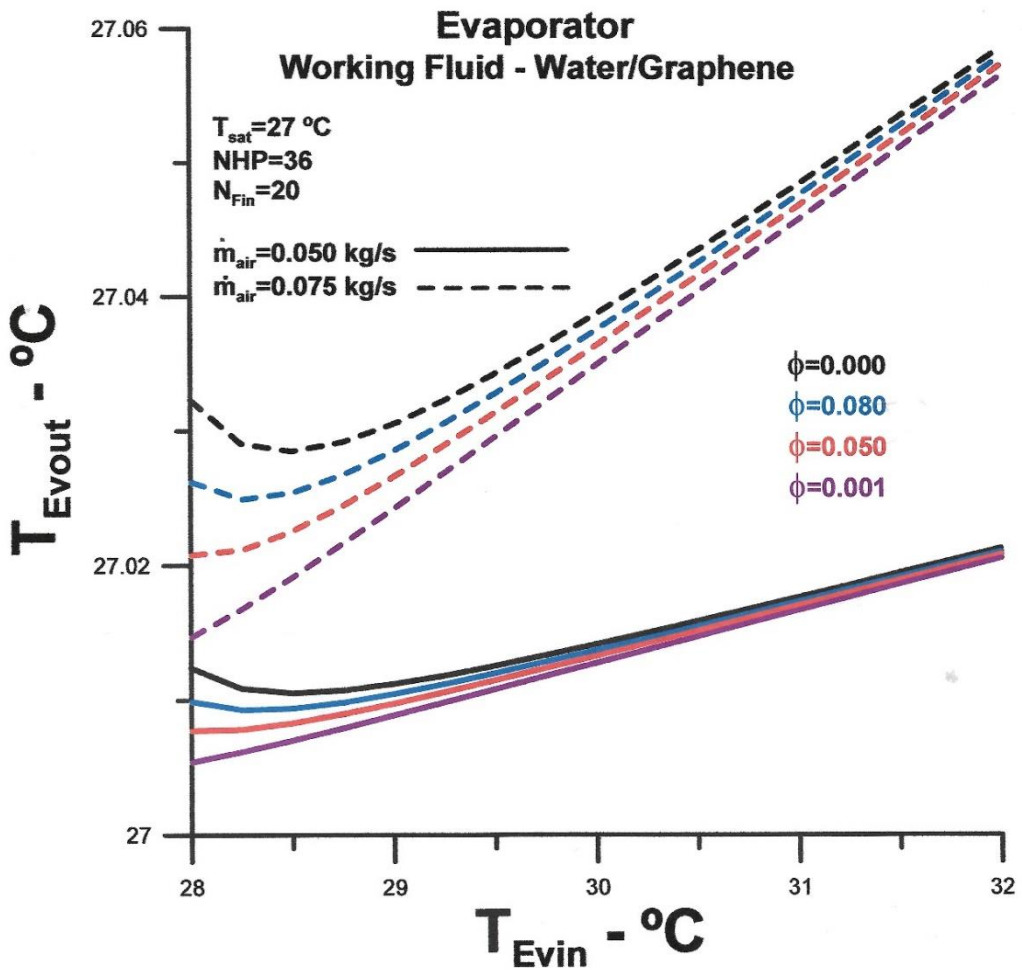

Figure 13: Outlet air temperature versus inlet air temperature for NHP=36 and N_{Fin}=20

CONCLUSION

The aim is to theoretically analyze the influence of the volume fraction of the nanofluid consisting of distilled water and graphene nanoparticles on the thermal performance of an evaporator made up of sets of heat pipes. The original evaporator uses distilled water as the working fluid and is part of a heat exchanger designed to work as an air conditioning system in operating rooms [1].

It is concluded that the nanofluid affects the heat exchange between the working fluid and the hot air entering the evaporator.

The most important conclusion of the performed analysis is that there is a volume fraction range for the nanofluid to work to improve the thermal performance of the heat exchanger. The results demonstrate that from a certain minimum value, there is greater heat exchange between the fluids until a certain volume fraction of the nanofluid is reached where the heat exchange is equal to the heat exchange of the original evaporator. Above this upper limit value in the volume fraction of the nanofluids, the heat exchange is lower than the heat exchange of the original evaporator.

According to the literature [1-15], many factors can lead to a high thermal resistance between the working fluid and the surface of the heat pipe, impairing the heat exchange. One is the deposition

of nanoparticles on the surface, and another, also feasible and related, is low pressure and the energy level involved in the process, that is, small heat exchangers are more affected.

REFERENCE

1. Ragil Sukarno, Nandy Putra1, Imansyah Ibnu Hakim, Fadhil Fuad Rachman, and Teuku Meurah Indra Mahlia (2021)." Multi-Stage Heat-Pipe Heat Exchanger for Improving Energy Efficiency of the HVAC System in a Hospital Operating Room." International Journal of Low-Carbon Technologies 2021, 16, 259–267. DOI:10.1093/ijlct/ctaa048

2. Nandy Putra, Trisno Anggoro, and Adi Winarta (2017). "Experimental Study of Heat Pipe Heat Exchanger in Hospital HVAC System for Energy Conservation." International Journal on Advanced Science Engineering and Information Technology Vol.7 (2017) No. 3. DOI: 10.18517/ijaseit.7.3.2135

3. Grzegorz Górecki, Marcin Łęcki, Artur Norbert Gutkowski, Dariusz Andrzejewski, Bartosz Warwas, Michał Kowalczyk and Artur Romaniak (2021). "Experimental and Numerical Study of Heat Pipe Heat Exchanger with Individually Finned Heat Pipes." Energies 2021, 14, 5317. https://doi.org/10.3390/en14175317

4. Hussam Jouhara, Sulaiman Almahmoud, Daniel Brough, Valentin Guichet, Bertrand Delpech, Amisha Chauhan, Lujean Ahmad, Nicolas Serey (2021). "Experimental and Theoretical Investigation of the Performance of an Air to Water Multi-Pass Heat Pipe-Based Heat Exchanger." Energy 219 (2021) 119624. https://doi.org/10.1016/j.energy.2020.119624

5. Khaled Elsaida, Mohamma Ali Abdelkareem, Hussein M. Maghrabie, Enas Taha Sayed, Tabbi Wilberforce, Ahmad Baroutaji, A.G. Olabi (2021). "Thermophysical Properties of Graphene-Based Nanofluids." International Journal of Thermofluids 10 (2021) 100073. https://doi.org/10.1016/j.ijft.2021.100073

6. Ali, N. (2022). "Graphene-Based Nanofluids: Production Parameter Effects on Thermophysical Properties and Dispersion Stability". Nanomaterials 2022, 12, 357. https://doi.org/10.3390/nano12030357

7. A. Kamyar, K.S. Ong, R. Saidur (2013). "Effects of Nanofluids on Heat Transfer Characteristics of a Two-Phase Closed Thermosyphon." International Journal of Heat and Mass Transfer 65 (2013) 610–618. http://dx.doi.org/10.1016/j.ijheatmasstransfer.2013.06.046

8. Agnieszka Kujawska, Robert Mulka, Samah Hamze, Gaweł Żyła, Bartosz Zajaczkowski, Matthias H. Buschmann, Patrice Estelle (2021). "The Effect of Boiling in a Thermosyphon on Surface Tension and Contact Angle of Silica and Graphene Oxide Nanofluids." Colloids and Surfaces A: Physicochemical and Engineering Aspects, Volume 627, 20 October 2021, 127082. https://doi.org/10.1016/j.colsurfa.2021.127082

9. Amir Akbari, Erfan Mohammadian, Seyed Ali Alavi Fazel, Mehdi Shanbedi, Mahtab Bahreini, Milad Heidari, and Goodarz Ahmadi (2019). "Comparison between Nucleate Pool Boiling Heat Transfer of Graphene Nanoplatelet- and Carbon Nanotube- Based Aqueous Nanofluids." ACS Omega 2019, 4, 19183−19192. DOI: 10.1021/acsomega.9b02474

10. Jacqueline Barber, David Brutin, and Lounes Tadrist (2011). "A Review on Boiling Heat Transfer Enhancement with Nanofluids." Nanoscale Research Letters 2011, 6:280. http://www.nanoscalereslett.com/content/6/1/280

11. K. N. Shukla A. Brusly Solomon, B. C. Pillai, and Mohammed Ibrahim (2010). "Thermal Performance of Cylindrical Heat Pipe Using Nanofluids." Journal of Thermophysics and Heat Transfer · October 2010. https://doi.org/10.2514/1.48749

12. Kapilan Natesan, Shashikantha Karinka (2023). "A Comprehensive Review of Heat Transfer Enhancement of Heat Exchanger, Heat Pipe and Electronic Components Using Graphene." Case Studies in The1mal Engineering 45 (2023) 10287 4. https:/ / doi.org/10.1 ol 6/ j.csite.2023.10287 4

13. Mohammed Salah Hameed, Abdul Rahman Khan, A. A. Mahdi (2013). "Modeling a General Equation for Pool Boiling Heat Transfer." Advances in Chemical Engineering and Science, 2013, 3, 294-303. http://dx.doi.org/10.4236/aces.2013.34037

14. A. Suriyawong, A. S. Dalkilic, and S. Wongwises (2012). "Nucleate Pool Boiling Heat Transfer Correlation for TiO2-Water Nanofluids." Journal of ASTM International, Vol. 9, No. 5. https://www.researchgate.net/publication/254200345

15. Nogueira, E. (2020). "Thermal performance in heat exchangers by the irreversibility, effectiveness, and efficiency concepts using nanofluids." Journal of Engineering Sciences, Vol. 7(2), pp. F1–F7. Doi: 10.21272/jes.2020.7(2).f1

16. Élcio Nogueira (2022). "Thermo-Hydraulic Optimization of Shell and Externally Finned Tubes Heat Exchanger by the Thermal Efficiency Method and Second Law of Thermodynamics." International Journal of Chemical and Process Engineering Research, 2022 Vol. 9, No. 1, pp. 21-41. DOI: 10.18488/65. v9i1.3130

17. Élcio Nogueira (2021). "Effects of R134a Saturation Temperature on a Shell and Tube Condenser with the Nanofluid Flow in the Tube Using the Thermal Efficiency and Effectiveness Concepts." World Journal of Nano Science and Engineering, 2021, 11, 1-24. https://doi.org/10.4236/wjnse.2021.111001

18. Warren M. Rohsenow (1951). "A Method of Correlating Heat Transfer Data for Surface Boiling of Liquids." Technical Report Nº 5, The Office Naval Research Contract N5ori-07827, Massachusetts Institute of Technology.